System Neglect and the Neurocomputational Substrates for Over- and Underreactions to Change

Mu-Chen Wang[1*]

George Wu[2]

Shih-Wei Wu[1,3*]

1. Institute of Neuroscience, National Yang Ming Chiao Tung University, Taipei, Taiwan

2. Booth School of Business, University of Chicago, Chicago, USA

3. Brain Research Center, National Yang Ming Chiao Tung University, Taipei, Taiwan

Corresponding Authors

Mu-Chen Wang <raccoon65.ym@nycu.edu.tw> or Shih-Wei Wu <sww@nycu.edu.tw>

ABSTRACT

The world constantly changes. Regime shifts are a particular kind of changes where the state of the world abruptly shifts from one to another. The ability to detect regime shifts, such as change in the state of a pandemic, markets, or inflation, significantly impacts our decisions and future. However, a change in regime is often not obvious, as the signals we receive are noisy and susceptible to the volatility of the environment. We designed a novel fMRI paradigm that extracts these important features in regime-shift detection. Human participants showed systematic over- and underreactions to change: Overreactions were most commonly seen when the signals are noisy but when the environments are stable where change is possible but unlikely. By contrast, underreactions were observed when the signals are precise but when the environments are unstable. These behavioral signatures are consistent with *system neglect* – individuals respond primarily to the signals and secondarily to the system that produces the signals. We found that system neglect arises from dissociable patterns of selectivity in two distinct brain networks. While a frontoparietal network (FPN) selectively represented individuals' degree of neglecting signal noise but not environment volatility, the ventromedial prefrontal cortex (vmPFC) showed the opposite pattern. Given that system neglect exists in many different domains of judgments, these results suggest that network-level parameter selectivity is a general organizing principle that gives rise to human judgment biases.

INTRODUCTION

Judging whether the world has changed is ubiquitous, from public health officials grappling with whether a COVID-19 surge has peaked, central banks figuring out whether inflation is easing, investors discerning whether the electric car market is getting traction, or romantic partners divining whether a relationship has soured. In some cases, epidemiological or statistical models provide guidance. However, in many, if not most cases, determinations of whether a regime shift has occurred are made intuitively (Sanders & Manrodt, 2003).

We investigate intuitive judgments of regime-shift detection using a simple empirical paradigm (Massey & Wu, 2005; Seifert et al., 2023). Although this paradigm abstracts some complications of real-world change detection, it maintains the most central features of the problem: regime-shift judgments are largely based on the *signals* from the environment and knowledge about the *system* that produces the signals. Inflation rate, COVID-19 cases, and sales of electric cars in recent months are all examples of signals. When COVID-19 cases continue to decline in recent weeks, one might infer a shift from COVID-19 to non-COVID-19 regime, only to find out a few weeks later a resurgence in cases. Indeed, signals such as recent COVID-19 cases are never precise indications of the true state of the world. By and large, signals are noisy. The noisier the signals are, the less *diagnostic* they are of the true regime. Further, signals are affected by how likely the regime shifts from one to another (transition probability). These two fundamental features, the diagnosticity of the signals and transition probability, can be conceptualized as two independent parameters of the system that generates the signals. We therefore refer to them as the *system parameters*. Previous works on regime shift found that people tend to overreact to change when they receive noisy signals (low signal diagnosticity) but nonetheless are in a stable environment (small transition probability). By contrast, underreactions to change were found when people receive precise signals (high signal diagnosticity) and are in an unstable environments (large transition probability) (Massey & Wu, 2005). These biases indicate *system neglect* – people respond primarily to the signals and secondarily to the system that produces the signals. System neglect is not only observed in regime-shift judgments, but also in other domains such as demand forecasting (Kremer et al., 2011), pricing decisions (Seifert et al., 2023).

At the neurobiological level, change detection was investigated in sensory

perception, reinforcement learning, and decision making. In sensory perception, change detection and change blindness are studied in tasks that asked the subjects to report the occurrence or nonoccurrence of change between two successively presented sensory stimuli (Beck et al., 2006; Beck et al., 2001; Gutteling et al., 2013; Huettel et al., 2001; Pessoa & Ungerleider, 2004; Reddy et al., 2006; Rensink, 2002; Sabri et al., 2005). Activity in the lateral prefrontal and parietal cortices were associated with the subjects' report of change regardless of whether a change actually occurred (Beck et al., 2001; Pessoa & Ungerleider, 2004). The odd-ball paradigm – where the presentation of occasional 'deviant' sensory (visual or auditory) stimuli along with standard stimuli – has also been widely used to investigate perceptual change detection. Using this paradigm, a key electrophysiological signature, the mismatch negativity (MMN) in electroencephalography (EEG) signals, has been identified (Naatanen et al., 1992). The MMN describes a negative deflection of event-related potential approximately 100-200ms after the appearance of the deviant stimulus. Using fMRI, activity in frontal, opercular, and insular cortices were found to represent the detection of the oddball stimuli (Hedge et al., 2015; Warbrick et al., 2009).

In reinforcement learning and decision making, the reversal-learning paradigm was often used to study the detection of change in the reward and/or punishment contingencies. The orbitofrontal cortex (OFC), striatum, and to a lesser degree, the medial prefrontal cortex and amygdala, were shown to be involved reversal learning (Izquierdo et al., 2017). OFC lesions in monkeys caused the animals to switch their choices between options more frequently following the reversal of reward contingencies, even though the ability to track local changes in reward rate remained intact (Walton et al., 2010). This result led to the hypothesis that OFC is involved in credit assignment (attributing the cause of reward outcomes to the chosen/appropriate stimulus) and spurred a series of investigations on the neurocomputational substrates for credit assignment (Boorman et al., 2016; Boorman et al., 2013; Jocham et al., 2016; Takahashi et al., 2011; Wang et al., 2020; Wilson et al., 2014). Another recent development was the study of neural representations for higher-order statistics of change (volatility) associated with reward contingency where the anterior cingulate cortex (ACC) was shown to track volatility (Behrens et al., 2007; Soltani & Izquierdo, 2019).

Although these studies provided key insights into the neurobiological basis of change detection, the neural mechanisms that give rise to over- and underreactions to

regime shifts remain elusive. To address this question, we scanned human subjects using blood oxygen level-dependent (BOLD) functional magnetic resonance imaging (fMRI) while they performed a '*regime-shift'* task. The subjects' task was to make probability judgments on regime shifts based on the signals they received and information about the system parameters. We found that two brain networks, the vmPFC-striatum network and the frontoparietal network, were critically associated with regime-shift judgments. These networks have their own unique computational roles, with the vmPFC-striatum network involved in computing and updating the probability judgments, and the frontoparietal network in evaluating the strength of evidence and the base rate for regime shifts. Further, these two networks are involved in the over- and underreactions to change by exhibiting dissociable selectivity profiles to the system parameters. The frontoparietal network correlated with individual subjects' degree of neglecting the signal diagnosticity parameter but not transition probability, while the vmPFC showed the opposite selectivity patterns. Together, these results suggest two mechanistic principles – network-level computational specificity and parameter selectivity – for system neglect in regime-shift judgments. Given that system neglect exists in many different domains of judgments and decision making, we conjecture that these principles may serve as general organizing principles that gives rise to a wide array of human judgment biases.

RESULTS

In a *regime-shift* task (Fig. 1A), the subjects in each trial saw a series of sequentially presented sensory signals (red or blue balls). They were told that the signals came from one of two regimes, the red regime and the blue regime (Fig. 1B). Each trial started with the red regime, but can shift to the blue regime at any point in time during the trial. Each time the subjects saw a new signal, she or he had to provide estimate of the probability that the current regime was the blue regime. In other words, this probability estimate was equivalent to the probability estimate of regime shift. They were also instructed that, during a trial, once the regime has shifted from the red to the blue, the regime would remain in the blue regime until the end of the trial.

We manipulated two system parameters, transition probability and signal diagnosticity (Fig. 1C). Transition probability, Q, (possible values are 0.01, 0.05, and 0.1) specified the probability that the regime would shift from the red to the blue regime. Signal diagnosticity, D, (possible values at 1.5, 3, and 9) was the degree to which the two regimes differed. For example, an environment with high signal diagnosticity (e.g., D=9) indicates that there are 9 times more red balls than blue balls in the red regime and 9 times more blue balls than the red balls in the blue regime. Therefore, the weight that a signal (blue or red) carries for indicating which regime is the current regime depends on the level of signal diagnosticity (Fig. 1D): in a highly diagnostic environment, a blue signal very likely reveals a shift in regime. By contrast, in a low diagnostic environment, a blue signal most likely reflects no change in regime.

To establish the neural representations for regime-shift estimation, we performed three fMRI experiments (n=30 subjects for each experiment, 90 subjects in total). Experiment 1 was the main experiment, while Experiments 2 to 3 were the control experiments that ruled out two important confounds (Fig. 1E). Experiment 2 was designed to establish whether the results from Experiment 1 was truly about regime-shift estimation or simply reflected probability estimation (In Experiment 1, the subjects had to estimate the probability that the current regime is the blue regime). Experiment 2 was identical to Experiment 1 except that the environments were stationary (no transition from one regime to another was possible) in Experiment 2. Subjects in both experiments had to estimate the probability that the current regime is the blue regime, but only in Experiment 1 this estimation corresponds to the estimates of regime change. Therefore, activity that correlated with probability estimates in

Experiment 1 but not in Experiment 2 can be uniquely attributed to representing the probability estimates of regime shift. Experiment 3 was specifically designed to address the motor confounds—whether the neural signals correlated with the probability estimates arose from motor preparation and/or execution, as the subjects made button presses to enter their probability estimates. By comparing the fMRI results of these experiments, we were therefore able to establish the neural representations that can be uniquely attributed to the probability estimates of regime-shift.

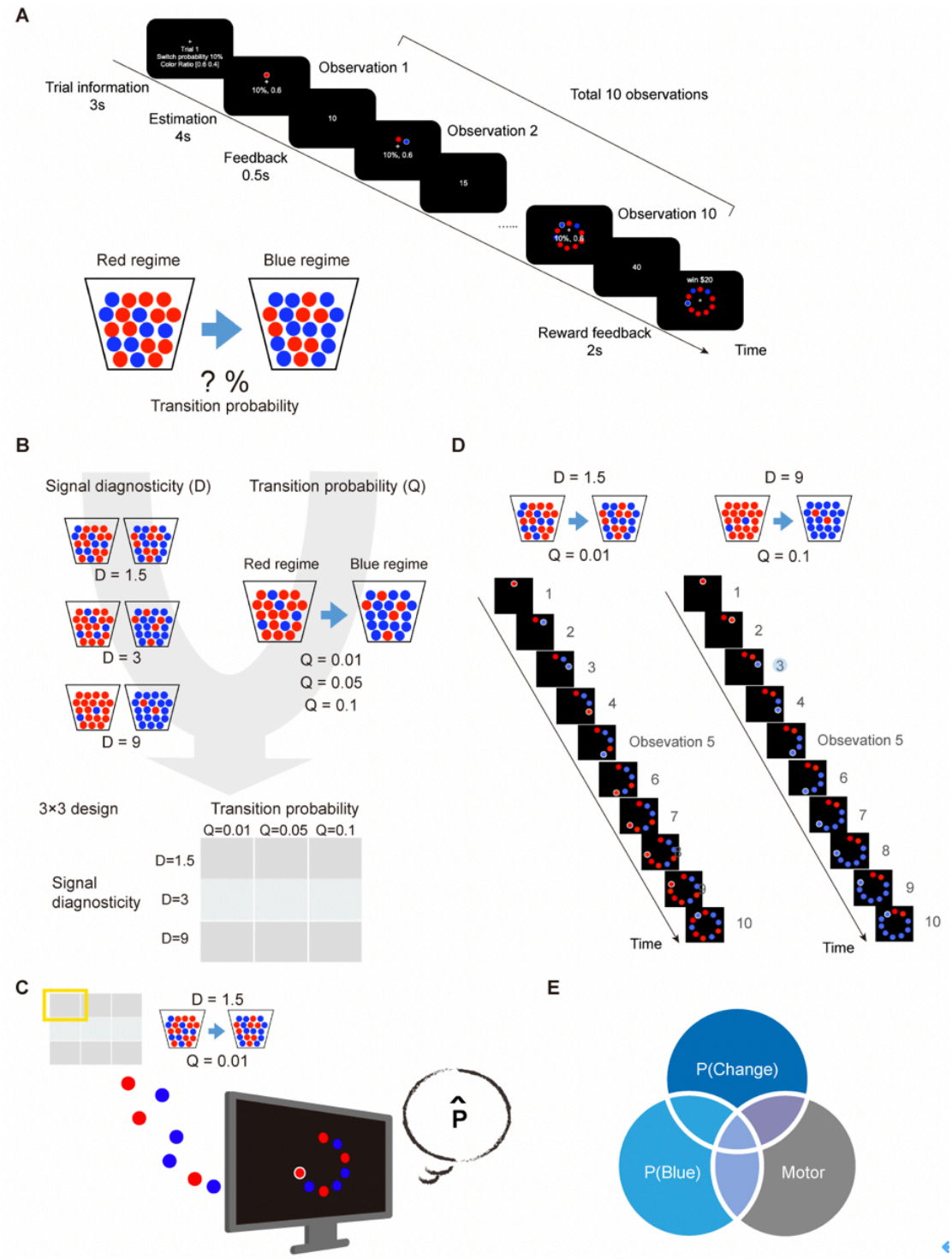

Figure 1. The regime-shift task. **A.** Trial sequence. The inset shows two example regimes. In this example, the number of red balls in the Red regime is three times the number of blue balls. For the Blue regime, the number of blue balls is three times the number of red balls. This is when the signal diagnosticity (*D*) is 3. In each trial, the subjects saw a sequence of red and blue signals and were told that these signals were drawn from one of the two regimes. Each trial always started at the Red regime but can shift to the Blue regime at any point

during a trial according to some transition probability (Q). **B.** Manipulation of the system parameters, i.e., transition probability (Q) and signal diagnosticity (D). We independently manipulated the Q (3 levels) and D (3 levels), resulting in a 3×3 factorial design. **C.** An example of a particular combination of the system parameters from the 3×3 design. Here the system that produces the signals has a 0.01 transition probability (Q) and 1.5 signal diagnosticity (D). Signals were sequentially presented to the subjects. When a new signal (observation) appeared, the subjects had to indicate probability estimate of regime shift. **D.** Two example trials sequences. The example on the left shows the sequence of 10 observations (blue and red signals) where the signal diagnosticity is 1.5 and the transition probability is 0.01. The example on the right shows the sequence of observations where the signal diagnosticity is 9 and transition probability is 0.1. In this example, the regime is actually shifted from the Red to the Blue regime at the third observation (observation 3 highlighted in light blue). **E.** We performed three fMRI experiments (30 subjects in each experiment) to investigate the neural basis of regime-shift judgments. Experiment 1 was the main experiment looking at regime shift—which corresponds to $P(Change)$ in the Venn diagram—while Experiments 2 and 3 were the control experiments that ruled out additional confounds. In both Experiments 1 and 2, the subjects had to estimate the probability that signals came from the blue regime. But unlike Experiment 1, in Experiment 2, which corresponds to $P(Blue)$, no regime shift was possible. In Experiment 3, the subjects were simply asked to enter a number with a button-press setup identical to Experiments 1 and 2. Therefore, Experiment 3 (Motor) allowed to rule out motor confounds.

Behavioral evidence for over- and underreactions to change

The subjects in general responded to the manipulation of the system parameters. When the transition probability was larger, they gave larger probability estimates. When the signal diagnosticity was larger, they were more certain about their probability estimates by giving either very small or very large probability estimates (Supplementary Fig. 1).

To examine over- and underreactions to change, we compared the subjects' actual probability estimates with those predicted by the ideal Bayesian model (Fig. 2 A). More precisely, we compared changes in the subjects' probability estimates between successive observations ΔP_{actual} with changes predicted by the ideal Bayesian model. When $\Delta P_{actual} = \Delta P_{Bayesian}$, the subjects neither overreacted nor

underreacted. An overreaction is defined when $\Delta P_{actual} > \Delta P_{Bayesian}$, and an underreaction is defined when $\Delta P_{actual} < \Delta P_{Bayesian}$. We therefore referred $\Delta P_{actual} - \Delta P_{Bayesian}$ as an Index of Overreaction (*IO*). Here we found that the subjects tended to overreact to change ($IO > 0$) when they received noisy signals (due to low signal diagnosticity) and when they were in stable environments (small transition probability). By contrast, underreactions ($IO < 0$) were most commonly observed when they were in unstable environments (larger transition probability).

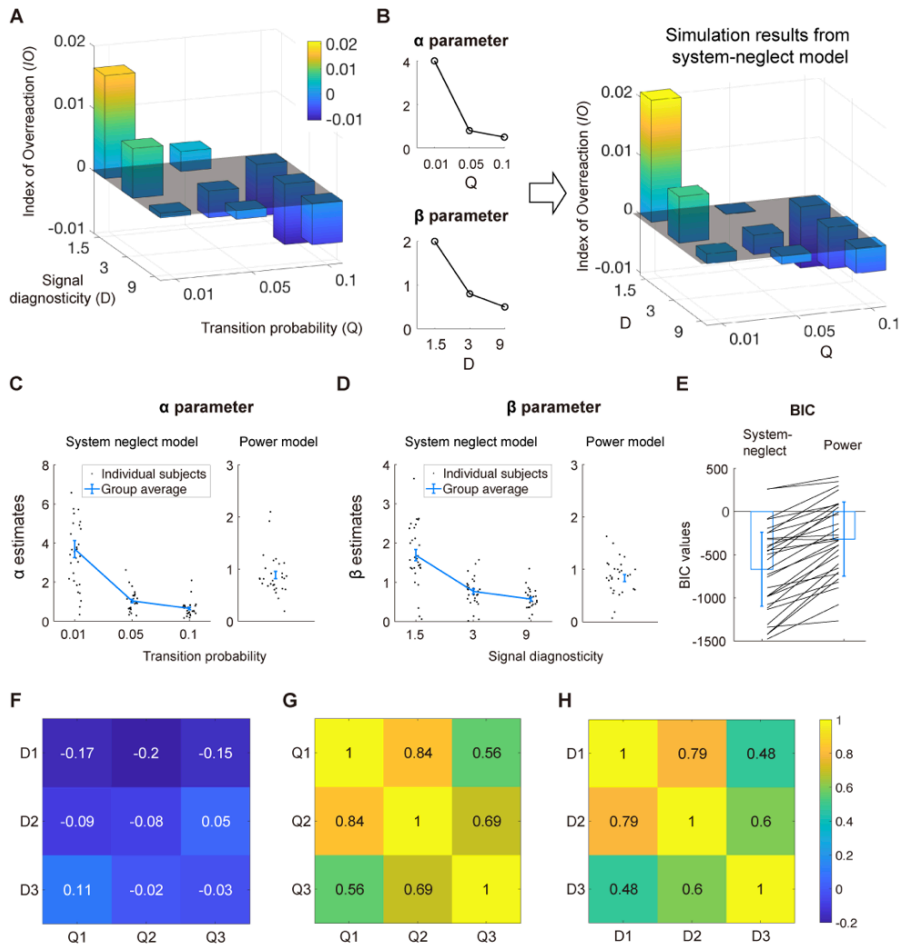

Figure 2. Behavioral results. **A.** Over- and underreactions to change. The median Index of Overreaction (*IO*) (across all subjects) is plotted as a function of transition probability and signal diagnosticity. Subjects overreacted to change when *IO* is greater than 0, underreacted when *IO* is smaller than 0. *IO* is computed by comparing the subjects' actual change in probability estimates between two successive observations with those predicted by the ideal Bayesian model. **B.** System-neglect model predictions of over- and underreactions to change. We simulated probability estimates of regime-shift based on the system-neglect model with parameters (α and β) set at the values shown on the left. The α and β parameters were the

weighting parameter respectively assigned to transition probability (Q) and signal diagnosticity (D). The simulated probability estimates were based on the sequence of stimuli the actual subjects experienced in the experiment. Through the Index of Overreaction, the simulated data revealed patterns of over- and underreactions to change similar to the patterns in the real data shown in 2A. **C-D.** Parameter estimates of the system-neglect model and power model. **C.** Weighting parameter for transition probability (α parameter). **D.** Weighting parameter for signal diagnosticity (β parameter). **E.** Model comparison. We plot the Bayesian Information Criterion (BIC) of the system-neglect model and the power model. The bars indicate the mean BIC averaged across subjects. Each black line represents a single subject. Error bars represent ± 1 standard error of the mean. Lower BIC values indicate better models. **F-H.** Sensitivity to transition probability and signal diagnosticity are independent. **F.** Pearson correlation coefficients of the subjects' α (sensitivity to transition probability) and β (sensitivity to signal diagnosticity) parameter estimates between different levels of transition probability (Q1 to Q3) and signal diagnosticity (D1 to D3). All pairwise correlations were not significantly different from 0 (p>0.05). **G.** Correlations of the α parameter estimates between different levels of transition probability. All pairwise correlations were significantly different from 0 (p<0.05). **H.** Correlations of the β parameter estimates between different levels of signal diagnosticity. All pairwise correlations were significantly different from 0 (p<0.05).

These patterns of over- and underreactions were consistent with the system-neglect hypothesis (Massey & Wu, 2005; Seifert et al., 2023). In essence, system neglect describes the tendency to respond primarily to the signals and secondarily to the system that generates the signals. In the context of this experiment, the system-neglect hypothesis predicts overreactions to change when the subjects receive noisy signals (due to low signal diagnosticity) but are nonetheless in stable environments (small transition probability). For example, a subject overreacts by increasing probability estimates of change when seeing a blue signal knowing full well that the red regime has many blue balls as well (low signal diagnosticity) and that the transition probability was very small. By contrast, the system-neglect hypothesis predicts underreactions when the subjects receive more precise signals (due to high signal diagnosticity) and when they are in unstable environments (large transition probability). For example, knowing that the environment is very unstable and the regimes are drastically different (low signal diagnosticity: red regime contain mostly

red balls, blue regime contain mostly blue balls), the subject underreacts to a blue signal by not changing enough her probability estimates simply because she has seen some red signals in the recent past.

To quantitatively describe these over- and underreactions to change, we developed two models, system-neglect model and the power model (see Methods for details). The two models are parameterized versions of the ideal Bayesian model that allow distortion of transition probability and signal diagnosticity through implementing a weighting parameter for transition probability (α parameter) and for signal diagnosticity (β parameter). In short, α reflects distortion of transition probability because $\alpha \times q$ in the system-neglect model represents the decision maker's belief about transition probability (q). For example, when $\alpha = 4$ and $q = 0.01$, the decision maker overreacts to a 0.01 transition probability as if it were 0.04. By contrast, β controls the extent to which the decision maker overweighs or underweighs signal diagnosticity (d^{β}) when a piece of evidence (the blue or red signals the subjects saw) is presented to the subjects. For example, when $\beta = 2$ and signal diagnosticity $d = 1.5$, the subjects would treat seeing a blue signal as if it had a 1.5^2 to 1 odds in favor of change rather than a 1.5 to 1 odds. For details of the system-neglect model, see *Methods*. In the system-neglect model, we estimated the weighting parameters separately at each level of transition probability and signal diagnosticity. In Fig. 2B, we show predictions of the α and β parameters in the system-neglect model that leads to patterns of over- and underreactions to change similar to those observed in the real data (Fig. 2A). That is, using exactly the same sequences of stimuli that all the subjects in the experiment saw, we simulated a decision maker's probability estimates using the system-neglect model with the α and β parameters set at the values shown in Fig. 2B. Based on the simulated probability estimates, we computed and show the Index of Overreaction (IO).

In contrast to the system-neglect model, the power model estimated the weighting parameter across different levels so that there is one α parameter estimate and one β parameter estimate. The power model therefore can only predict *overall* over- and underreactions to change (across different levels of transition probability or signal diagnosticity; Fig. 2B for an example prediction of the power model). Note that when the value of these parameters is 1, the two quasi-Bayesian models are equivalent to the ideal Bayesian model ($\alpha = 1$ and $\beta = 1$ across all levels; lines labeled as ideal Bayesian in Fig. 2B). Finally, we show that a decision maker who

completely ignores the system parameter and therefore is defined by $\alpha_1 Q_1 = \alpha_2 Q_2 = \alpha_3 Q_3$ and $\beta_1 D_1 = \beta_2 D_2 = \beta_3 D_3$. In this experiment, $\alpha_1 \times 0.01 = \alpha_2 \times 0.05 = \alpha_3 \times 0.1$ and $\beta_1 \times 1 = \beta_2 \times 3 = \beta_3 \times 9$. In Fig. 2B, we also show an example prediction of the complete-neglect decision maker.

For each subject separately in Experiment 1, we fit these two models to the probability estimates. For the system-neglect model, the model fits indicated that subjects overweight small transition probability but underweight large transition probability (Fig. 2CD). The mean α estimate was 3.69, 1.04 and 0.65 respectively for 0.01, 0.05, 0.1 transition probabilities. This suggested that, on average, when transition probability was 0.01, subjects on average treated as if it were 0.0369. By contrast, when transition probability was 0.1, the subjects on averaged treated it as if it were 0.065. A factor of 10 difference (0.01 and 0.1) became less than a factor of 2 (0.0369 and 0.065). For signal diagnosticity, the mean parameter estimates of β were 1.69, 0.77 and 0.57 respectively for 1.5, 3, and 9 signal diagnosticity. This suggested that subjects overweight small diagnosticity but underweight large diagnosticity. Together, large parameter estimates ($\alpha > 1, \beta > 1$) at low signal diagnosticity (noisy signals) and low transition probability (stable environments) explained overreactions to changes, while small parameter estimates ($\alpha < 1, \beta < 1$) at large signal diagnosticity (precise signals) and large transition probability (unstable environments) explained underreactions to change. For the power model, the fits suggest that the subjects slightly underweighted both the transition probability and signal diagnosticity, which clearly did not capture over- and underreactions to change. The mean α and β estimates were 0.89 and 0.83 respectively. Model comparison using Bayesian information criterion (BIC) further revealed that the system-neglect model was indeed the better model than the power model ($t(29) = 9.09$, $p < 0.01$). The BIC value was lower in the system-neglect model in 29 out of 30 subjects (Fig. 2E). Finally, fitting these two models to Experiment 2 yielded similar results (Supplementary Fig. 2).

Together, these results indicated that over- and underreactions to change arise from system neglect and replicated the findings by Massey and Wu (2005). Critically, the degree of system neglect (neglecting the system parameters) can be captured by the negative slope of the parameter estimate as a function of the system parameter levels (Fig. 2CD): the steeper the slope, the larger the system neglect. By contrast, when people are ideal Bayesian and show no system neglect, all the parameter

estimates would be 1 (because an ideal Bayesian does not overweight or underweight either the transition probability or signal diagnosticity) and the slope therefore would be 0.

Finally, we found no correlation between the α and β parameter estimates (Fig. 2E). This suggests that these two parameters indeed captured unique aspects of the subjects' probability estimation behavior. It also informs us that over- and underreactions are probably not a general personality trait: a person who overreacts to transition probability does not imply that she would also overreact to signal diagnosticity. There is, however, another interesting aspect of the data. Subjects who showed stronger weighting to a transition probability would also show stronger weighting at other transition probability levels (Fig. 2F). The same can be said about signal diagnosticity (Fig. 2G). This indicates that there is consistency in how a person treats a particular system parameter and suggests that we do have to look at over- and underreactions to change from the lens of the system parameters.

Ventromedial prefrontal cortex (vmPFC) uniquely represents regime-shift probability estimates

To investigate the dynamics of regime-shift estimation, we asked the subjects to provide probability estimate of regime shift at each observation. This allowed us to identify brain regions that correlated with the probability estimates of regime shift at the single observation level (see Fig. 3A with two examples). We found that the ventromedial prefrontal cortex (vmPFC), ventral striatum, and many other brain regions, including the motor, insular, occipital cortices, and the cerebellum significantly correlated with the regime-shift probability estimates (Fig. 3B; see GLM-1 in Methods). See Supplementary Table S1 to S3 for significant clusters of activation using Gaussian random field theory (S1), permutation test on threshold-free-cluster-enhancement statistic (S2), and permutations test on cluster-extent statistic (S3). To examine the robustness of the probability-estimate ($\hat{P}$) results, we ran a GLM that replaced the probability estimates with the log odds of probability estimates ($\log\left(\hat{P}/\left(1-\hat{P}\right)\right)$; Supplementary Fig. 3), a GLM (GLM-2 in Methods) that included regressors that contributed to $\hat{P}$ (Supplementary Fig. 4), and a GLM where we examined $\hat{P}$ separately on observations when the blue signal appeared and when the red signal appeared (Supplementary Fig. 5). We found that the vmPFC showed

significant negative correlation with probability estimates and the log odds of probability estimates, suggesting that the probability-estimate correlates in vmPFC were robust.

In order to rule out potential confounds and establish whether these regions truly represented regime-shift probability estimates, we performed identical analysis on Experiments 2 and 3. Like Experiment 1, the subjects in Experiment 2 also had to provide probability estimates that the current regime is the blue regime. However, unlike Experiment 1, in Experiment 2 there was no manipulation of regime shift. Hence, even though in both experiments the subjects estimated the probability that the current regime is the blue regime, only in Experiment 1 were these probability estimates meant to indicate regime-shift estimates. In Experiment 2, many brain regions found in Experiment 1, except for the vmPFC, ventral striatum, and the bilateral central opercular cortex extending to the insula, showed significant correlation with probability estimates (Fig. 3C). Information about significant clusters of activation from Experiments 2 and 3 can be seen in Supplementary Table S4 and S5 respectively.

Experiment 3 served as a control experiment for the motor confounds. The subjects in Experiment 3 were instructed to enter two-digit numbers shown on the screen in a task environment otherwise identical to both Experiments 1 and 2. Again, many brain regions found in Experiment 1, except for the vmPFC, ventral striatum, and the bilateral central opercular cortex extending to the insula, correlated with the instructed number (Fig. 3D). Together, these results suggested that, at the whole-brain level, the vmPFC, ventral striatum, and part of the operculum and insular cortex are uniquely associated with regime-shift probability estimates. ROI analyses on the vmPFC, ventral striatum, and the operculum/insula across the three experiments can be seen in the Supplement (Supplementary Fig. 6).

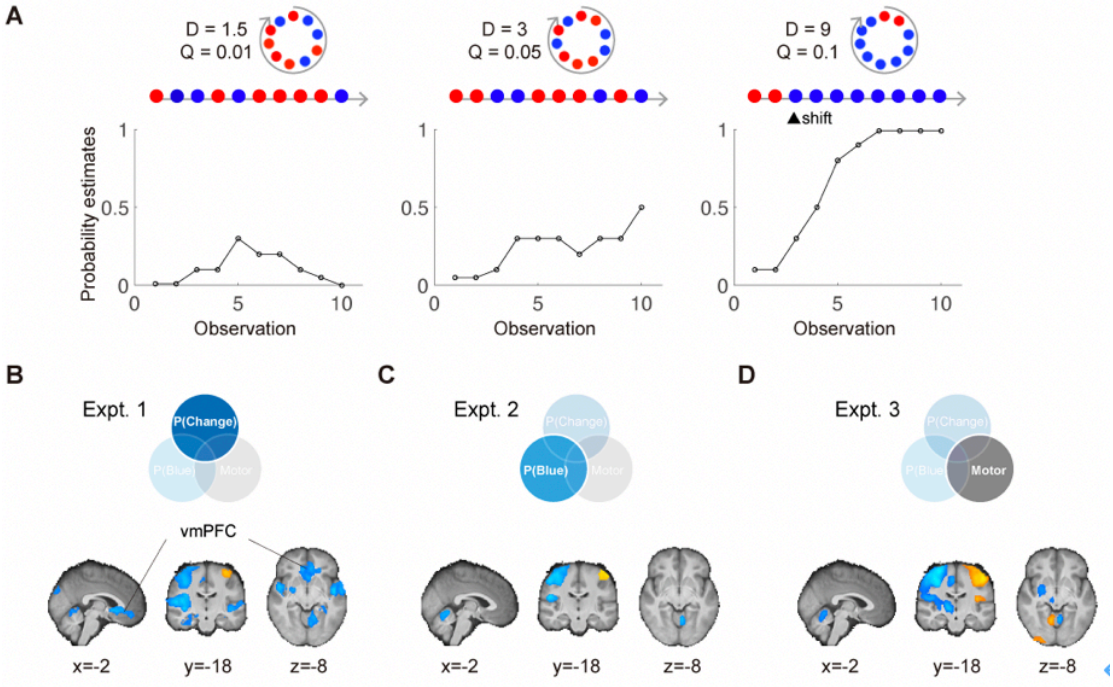

Figure 3. Neural representations for regime-shift probability estimates. **A.** Three examples of probability estimates. In each example, a subject's probability estimates are plotted as a function of the sequence of signals (blue or red balls) she or he observed, which are shown at the top of the graph. In the example on the right graph, the regime was actually shifted from the Red to the Blue regime at the third observation. **B.** Experiment 1: whole-brain results on activity that significantly and negatively correlated with the probability estimates of regime shift. **C.** Experiment 2: whole-brain results on activity that significantly and negatively correlated with the probability estimates that signals came from the Blue regime. **D.** Experiment 3: whole-brain results on activity that significantly and negatively correlated with the numbers the subjects were instructed to press using the button box.

Ventromedial prefrontal cortex and ventral striatum are involved in updating beliefs about regime shift

In addition to their involvement in estimating the probability of regime shifts, we also found that the vmPFC and ventral striatum were associated with the subjects' change in their beliefs about regime shift (Fig. 4; see GLM-2 in Methods and Supplementary Table S6 for significant clusters of activation). While many brain regions correlated with the regime-shift probability estimates, only these two regions also correlated with the change in beliefs about regime shift. Here the change in beliefs is captured

by the difference between two successive probability estimates (probability estimate at the current observation and the probability estimate at the previous observation; see Fig. 4A for an example). This suggested that there is an updating mechanism in the vmPFC and ventral striatum where beliefs about regime shift are updated at each new observation based on the probability estimates from the previous observation.

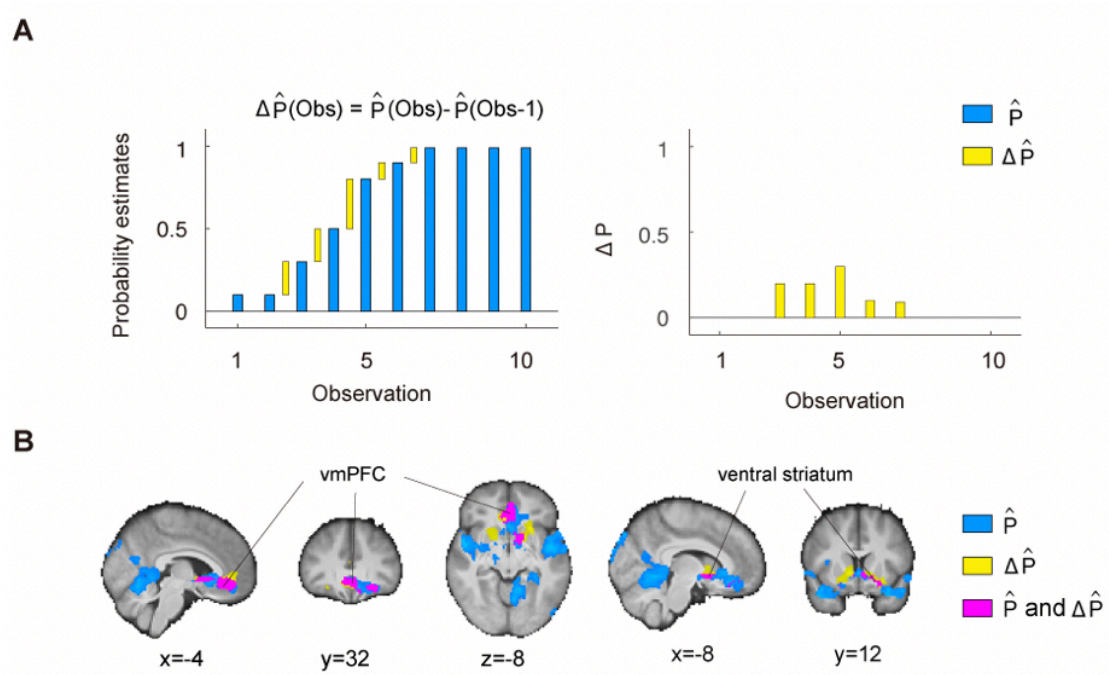

Figure 4. Neural representations for the updating of beliefs about regime shift. **A.** An example. Here updating is captured by the difference in probability estimates between two successive observations ($\Delta\hat{P}$). The Blue bars capture the current probability estimates ($\hat{P}$), while yellow bars capture $\Delta\hat{P}$. **B.** Whole-brain results showing significant brain regions that correlate with the updating of beliefs about change ($\Delta\hat{P}$). The clusters in yellow represent activity correlated with $\Delta\hat{P}$. The blue clusters represent activity correlated with the regime-shift estimates ($\hat{P}$). The magenta clusters represent the overlap between the two. vmPFC: ventromedial prefrontal cortex.

A frontoparietal network represents key variables for estimating regime shifts

But how did the subjects arrive at their regime-shift estimates? Clearly the subjects had to consider both the signals (blue or red balls) and the system parameters that are responsible for producing the signals. Simply relying on either is not enough to give accurate estimates. We therefore aimed to identify the neural representations for the key variables that contribute to regime-shift estimates. Guided by our theoretical

framework (both the Bayesian and quasi-Bayesian models), we focused on two variables—the interaction between signals and signal diagnosticity and dynamic base rate of change.

Our theoretical framework for regime-shift estimation makes two fundamental predictions. First, a signal should be weighted in favor of or against regime shift according to the signal diagnosticity: observing a blue ball in a highly diagnostic environment (e.g., signal diagnosticity is 9) should serve as strong evidence that the regime has shifted. By contrast, observing a blue ball when the red and blue regimes are very similar (e.g., signal diagnosticity is 1.5) tells us little about whether the regime has shifted. In other words, the signals the subjects received should directly interact with signal diagnosticity. Therefore, we code a blue signal as 1 and a red signal as -1. To model the interaction between the signal and signal diagnosticity, the signal code (1 or -1) was multiplied by the signal diagnosticity (two examples are shown in Fig. 5A). At the whole-brain level, we found that a frontoparietal network including the dorsal medial prefrontal cortex (dmPFC), lateral prefrontal cortex (bilateral inferior frontal gyrus, IFG), and the posterior parietal cortex (bilateral intraparietal sulcus, IPS) represented the interaction between the signals and signal diagnosticity (Fig. 5A). These brain regions overlapped with what is commonly referred to as the frontoparietal control network (Buckner et al., 2013; Seeley et al., 2007; Yeo et al., 2011).

The second prediction our theoretical framework offers is the base rate of regime shift. Specifically, the Bayesian model predicts that the base rate should increase over time (see two examples in Fig. 5B). To express the base rate of regime shift, we use the natural logarithm of the odds of regime shift, $\log(Q_t\ odds)$. Hence, log(D)×signal and $\log(Q_t\ odds)$ are the two key variables for estimating regime shifts. We found that most brain regions in the frontoparietal network that represented log(D)×signal also correlated with $\log(Q_t\ odds)$ (Fig. 5B; dmPFC: $t(29)=-1.69$, $p=0.10$, left IFG: $t(29)=-2.20$, $p=0.04$, right IFG: $t(29)=-2.64$, $p=0.01$, left IPS: $t(29)=-2.35$, $p=0.03$, right IPS: $t(29)$, $p=0.05$). By contrast, the brain regions identified to represent $\log(Q_t\ odds)$ did not correlate with log(D)×signal (Supplementary Fig. 7, which also included ROI results from vmPFC and ventral striatum). Together, these results suggest that the frontoparietal network is critically involved in representing these two key variables, log(D)×signal and $\log(Q_t\ odds)$, for estimating regime shift. See Supplementary Tables S6 to S8 for information about significant clusters of

activation using Gaussian random field theory (S6), permutation test on threshold-free-cluster-enhancement (TFCE) statistic (S7), and permutation test on cluster-extent statistic (S8).

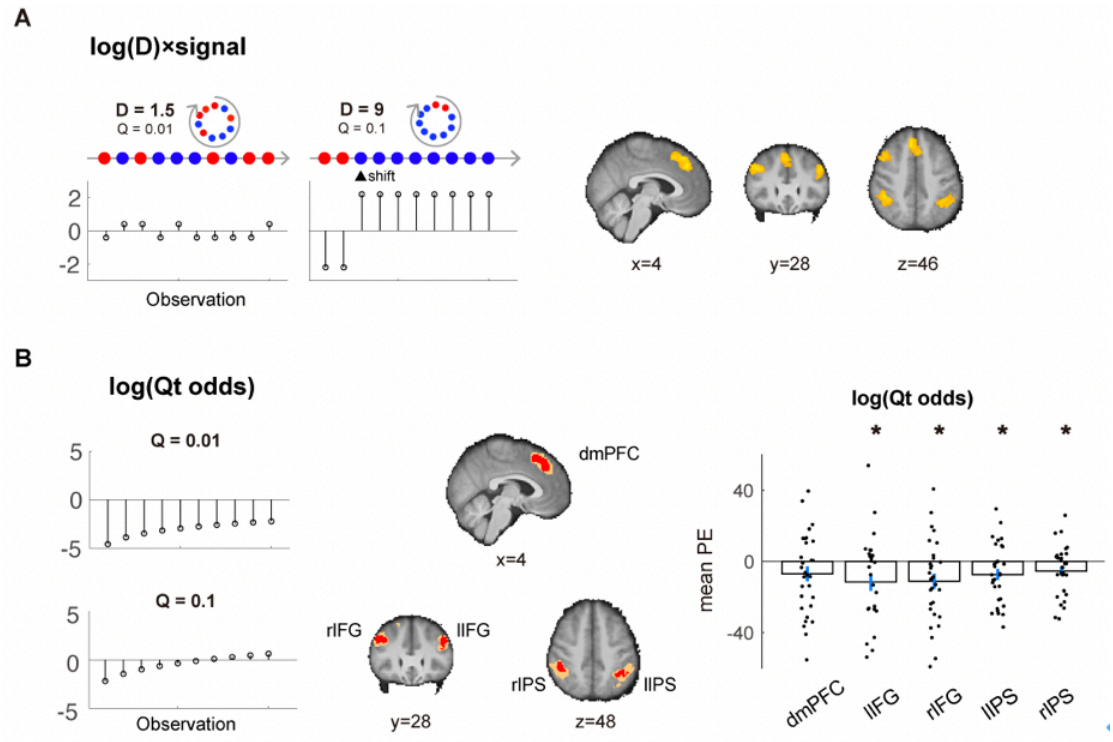

Figure 5. A frontoparietal network represented key variables for regime-shift computations. **A.** Variable 1: strength of evidence in favor of/against regime shifts. Here we use the interaction between the signals and the signal diagnosticity parameter as a measure of the evidence strength. Left: two examples of the interaction between signal diagnosticity and sensory signal. The *x*-axis represents the sequence of observations, from the first to the last observation, in a trial. The *y*-axis represents the interaction (the logarithm of signal diagnosticity×signal, or log(*D*)×signal). A blue signal is coded as 1 and a red signal is coded as -1. Right: whole-brain results showing brain regions in a frontoparietal network that significantly correlated with log(*D*)×signal. **B.** Variable 2: base rate of change ($\log(Qt\ odds)$. Two examples showing the dynamic nature of $\log(Qt\ odds)$ (left graphs). To examine the effect of $\log(Qt\ odds)$, we performed independent region-of-interest analysis (leave-one-subject-out, LOSO) on the brain regions identified to represent strength of evidence (5A). The ROI analysis examined the regression coefficients (mean PE) of $\log(Qt\ odds)$. The * symbol indicates $p<0.05$, ** indicates $p<0.01$. dmPFC: dorsomedial prefrontal cortex; lIPS: left intraparietal sulcus; rIPS: right intraparietal sulcus; lIFG: left inferior frontal gyrus; rIFG: right inferior frontal gyrus.

System neglect is associated with dissociable patterns of parameter selectivity between distinct brain networks

To further understand how the vmPFC-striatum and frontoparietal networks contributed to over- and underreactions to change, we next focused on examining whether and how they represented the individual differences in system neglect. First, we examined whether these brain networks show selective preference for a particular system parameter, which we refer to as *parameter selectivity*. That is, we considered the possibility that a brain network might selectively represent individual differences in the degree of neglecting one system parameter (e.g., transition probability) but not the other (e.g., signal diagnosticity). Second, we asked parameter selectivity is signal-dependent. By signal we meant the blue (a signal in favor of potential change) and the red (a signal against potential change) the subjects encountered. In other words, we asked whether the neural representations for the degree of neglect depend on which signal appeared to the subjects.

To examine these two properties, we performed psychometric-neurometric comparison analyses on the system parameters (transition probability Q and signal diagnosticity D). First, we define the behavioral measure of system neglect. To visualize this measure, we need to first consider two extreme decision makers, the ideal Bayesian and the complete neglect. In Fig. 6A (left graph), we use signal diagnosticity (D) as an example to illustrate the pattern of these two decision makers. The vertical axis is $\beta \log(D)$ and the horizontal axis is the signal-diagnosticity level (D). For the ideal Bayesian (open circles), since she does not overweight or underweight D, her β should always be 1. We can then define the *ideal Bayesian slope* by regressing $1 \times \log(D)$ against the diagnosticity level (1, 2 and 3). On the other hand, for a complete-neglect decision maker, since she completely neglects signal diagnosticity, $\beta_1 \log(D_1) = \beta_2 \log(D_2) = \beta_3 \log(D_3)$. Hence, the *complete-neglect slope* should be 0. These two slopes provide the boundaries for system neglect. For each subject, we computed $\beta \log(D)$ at each D level where β is his or her parameter estimate at that level according to the system-neglect model (Fig. 2D). We then estimated the slope – also referred to as the *behavioral slope* so as to distinguish it from the *neural slope* reported later – and used it as a measure of the degree of neglect. Since system neglect is in between complete neglect and ideal Bayesian, the closer a subject's slope to the complete neglect slope, the more she or

he neglected the system parameter. Therefore, the behavioral slope is a behavioral measure of the degree of system neglect. We have two such measures from each subject, one for the signal diagnosticity parameter (top row in Fig. 6A), and the other for the transition probability parameter (bottom row in Fig. 6A). The right graphs in Fig. 6A shows the behavioral slope of each subject (top: signal diagnosticity; bottom: transition probability).

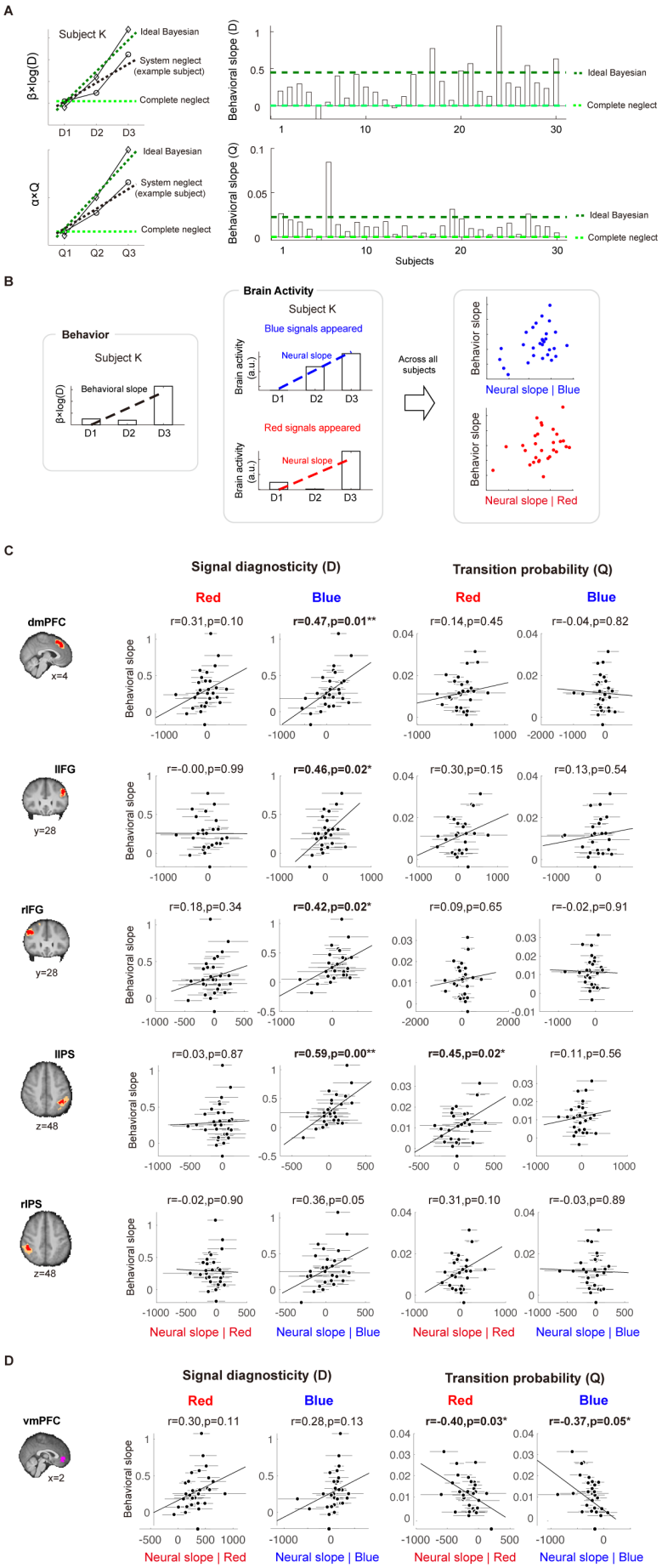
A
Subject K
Ideal Bayesian
System neglect (example subject)
Complete neglect
β×log(D)
D1 D2 D3
α×Q
Q1 Q2 Q3
Behavioral slope (D)
Behavioral slope (Q)
Subjects
B
Behavior
Behavioral slope
Brain Activity
Blue signals appeared
Neural slope
Red signals appeared
Brain activity (a.u.)
Across all subjects
Behavior slope
Neural slope | Blue
Neural slope | Red
C
Signal diagnosticity (D)
Transition probability (Q)
Red
Blue
dmPFC
x=4
lIFG
y=28
rIFG
lIPS
z=48
rIPS
Behavioral slope
r=0.31,p=0.10
r=0.47,p=0.01**
r=0.14,p=0.45
r=-0.04,p=0.82
r=-0.00,p=0.99
r=0.46,p=0.02*
r=0.30,p=0.15
r=0.13,p=0.54
r=0.18,p=0.34
r=0.42,p=0.02*
r=0.09,p=0.65
r=-0.02,p=0.91
r=0.03,p=0.87
r=0.59,p=0.00**
r=0.45,p=0.02*
r=0.11,p=0.56
r=-0.02,p=0.90
r=0.36,p=0.05
r=0.31,p=0.10
r=-0.03,p=0.89
Neural slope | Red
Neural slope | Blue
D
vmPFC
x=2
r=0.30,p=0.11
r=0.28,p=0.13
r=-0.40,p=0.03*
r=-0.37,p=0.05*

Figure 6. System neglect is associated with network-level parameter selectivity. **A.** Estimating the degree of system neglect. For each system parameter, we plot the subjectively weighted system parameter against the system parameter level (top row: signal diagnosticity; bottom row: transition probability). For each subject, we estimated the slope (how subjectively weighted system parameter changes as a function of parameter level) and used it as a behavioral measure of system neglect (behavioral slope). We also show an ideal Bayesian (no system neglect) decision maker's slope (dark green) and the slope of a decision maker who completely neglects the system parameter (in light green; the slope would be 0). A subject with stronger neglect would have a behavioral slope closer to complete neglect. **B.** Psychometric-neurometric comparison on system neglect. For each system parameter, we regressed neural activity of a ROI against the parameter level and used the slope estimate as a neural measure of system neglect (neural slope). We estimated the neural slope separately for blue-signal observations (when the subject saw a blue signal) and red-signal observations. We computed the Pearson correlation coefficient (r) between the behavioral slope and the neural slope and used it to statistically test whether there is a psychometric-neurometric match. **C.** The frontoparietal network selectively represented individuals' degree of neglecting the signal diagnosticity parameter, but not the transition probability parameter. In particular, the frontoparietal network represented signal-diagnosticity neglect only when a signal in favor of potential change (blue) appeared: all the regions except the right IPS showed statistically significant psychometric-neurometric match. By contrast, regardless of the signals, the frontoparietal network did not show significant psychometric-neurometric match on the transition-probability parameter. **D.** The vmPFC selectively represented individuals' degree of neglecting the transition-probability parameter (r=-0.4, p=0.03 when red appeared; r=-0.37, p=0.05 when blue appeared), but not the signal-diagnosticity parameter (r=0.3, p=0.11 when red appeared; r=0.28, p=0.13 when blue appeared). Error bars represent ± 1 standard error of the mean.

For the neural data, we defined a neural measure of system neglect similar to how we defined the behavioral measure of system neglect. Using the signal diagnosticity parameter as an example, for a particular ROI, we used its average activity at each diagnosticity level as data and regressed them against the diagnosticity level. The slope estimate, referred to as the *neural slope*, from this linear regression gave us a neural measure of system neglect. To investigate whether the neural response differed between the blue (potential change) and red (no change)

signals, we separately estimated the neural slope when the subject encountered the blue signal and the red signal. We then computed the Pearson correlation coefficient between the behavioral slope and neural slope across all subjects.

We found that the vmPFC-striatum network and frontoparietal network showed clear dissociations in how they preferred the system parameters. First, the frontoparietal network represented individual subjects' degree of neglecting the signal diagnosticity parameter, but not the transition probability parameter (Fig. 6B). Notably, the regions within the frontoparietal network exhibited remarkable consistency in its parameter selectivity. In particular, when a signal in favor of change appeared (the blue signal), all regions except the right IPS within the frontoparietal network significantly correlated with individual subjects' degree of neglecting the diagnosticity parameter. By contrast, when a signal against potential change (red signal) appeared, all regions within the frontoparietal network did not significantly correlate with signal-diagnosticity neglect.

Second, in contrast to the frontoparietal network, the vmPFC selectively represented individual subjects' degree of neglecting the transition probability parameter but not the signal diagnosticity parameter (Fig. 6C). Further, unlike the frontoparietal network, the vmPFC did not show signal-dependent selectivity: it represented transition-probability neglect regardless of whether the blue or red signals appeared. For the ventral striatum, we found that it did not show selectivity to either the transition probability or signal diagnosticity parameter (Supplementary Fig. 8). Therefore, only the vmPFC in the vmPFC-striatum network showed parameter selectivity.

The above analyses suggest that the frontoparietal network and the vmPFC must communicate during regime shift estimation. In particular, when there is a signal for potential change, the frontoparietal network, responsible for estimating likelihood of change, must pass on this information to the vmPFC. We found that evidence the vmPFC and the frontoparietal network were interacting and that the magnitude of interaction was signal-dependent. When the blue signals appeared, vmPFC and the frontoparietal network were more strongly coupled, showing an increase in functional connectivity compared with when the red signals appeared (Fig. 7). This is consistent with the notion that, at the time a signal in favor of potential change appeared, information about the strength of evidence in favor of change is communicated from

the frontoparietal network to the vmPFC, which is involved in updating the regime-shift probability estimates (Fig. 4).

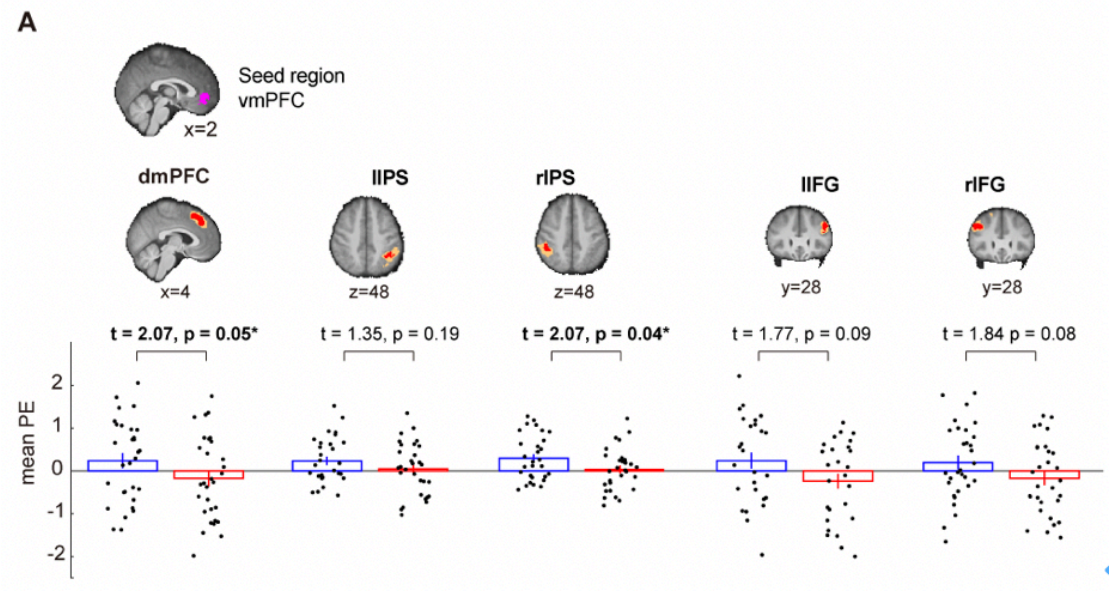

Figure 7. Functional coupling between the ventromedial prefrontal cortex (vmPFC) and frontoparietal network. To investigate whether the functional coupling between vmPFC and frontoparietal network changed depending on the signals (blue: signals in favor of change; red: signals against potential change) presented to the subjects, we used vmPFC as the seed region and performed a psycho-physiologic interaction (PPI) analysis. Two PPI contrasts were examined, namely the interaction between vmPFC response and presence of the blue signals, and the interaction between vmPFC response and the presence of the red signals. The mean parameter estimate (mean PE) of these two contrasts were plotted for each region in the frontoparietal network. Data points in black represent individual subjects' data. Error bars represent ± 1 standard error of the mean.

Neural-inspired behavioral analysis

Our neural results on network-level parameter selectivity further inspired a new behavioral analysis. From Fig. 6, it is clear that the frontoparietal network selectively represented individual subjects' degree of neglecting the signal-diagnosticity parameter only when the blue signal appeared. However, it remains unclear at the behavioral level whether the signal-diagnosticity neglect is primarily driven by the blue signal because the system-neglect model does not incorporate such possibility

when estimating neglect. To address this question, we reanalyzed the subjects' probability estimates data. We hypothesize that if signal-diagnosticity neglect occurred only when the blue signal appeared, the extent to which the probability estimates changed as a function signal diagnosticity would correlate with the behavioral slope only when the blue signal appeared but not when the red signal appeared. Indeed, this is what we found. Only when the blue signal appeared did the subjects' probability estimates reflected his or her degree of neglecting the signal diagnosticity parameter (Fig. 8A).

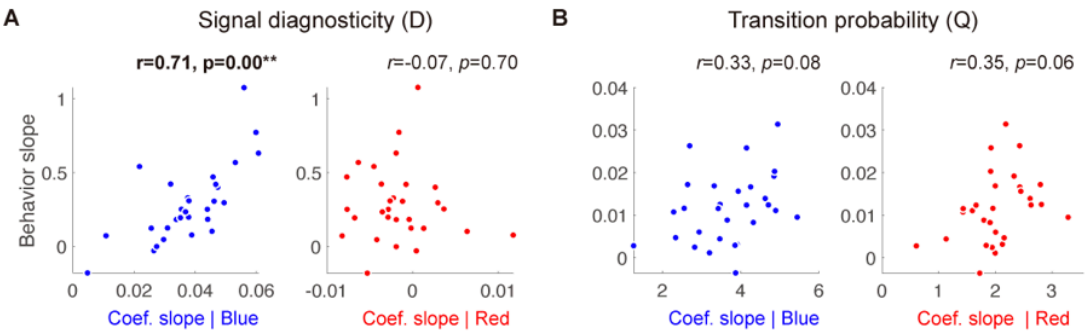

Figure 8. Neural-inspired behavioral analysis. We reanalyzed the subjects' probability estimates data by separately estimating how system parameters impacted probability estimates when the subjects received a blue signal (signal in favor of potential change) and when they received a red signal (signal against potential change). Using the subjects' probability estimates, we estimated the degree to which probability estimates changed as a function of the system parameter separately for the observations when the blue signals appeared (Coef. slope | Blue) and when the red signals appeared (Coef. slope | Red). **A.** Signal diagnosticity parameter. Pearson correlation (r) between behavioral slope and Coef. slope and its p-value for the blue (left graph) and red signal (right graph). **B.** Transition probability parameter. Pearson correlation (r) between behavioral slope and Coef. slope and its p-value for the blue (left graph) and red signal (right graph).

For the transition-probability neglect, results from the vmPFC indicates that transition-probability neglect manifests regardless of whether the signals are red or blue. Indeed, this is also what we found in the subjects' probability estimates. The subjects' probability estimates (marginally) reflected his or her transition-probability neglect when either the red or the blue signals appeared (Fig. 8B). Finally, we note that this is not a circular analysis. When we estimated the α and β parameters in the

system-neglect model (the crucial component for how the behavioral slope was estimated), we did not consider the possibility that these parameters can be affected differently depending on whether the subjects received a blue signal or a red signal. Therefore, this analysis further revealed a new insight: signal-diagnosticity neglect primarily came from the blue signal, while transition-probability neglect came from both the blue and red signals.

DISCUSSION

In this study, we investigated the neurocomputational mechanisms for regime-shift detection. Regime shifts are a particular kind of changes where the true state of the world shifts from one to another. Regime shifts are present in many daily situations, from the stock market (a change from the bull to the bear market) to the state of a pandemic. Detecting regime shifts can be challenging for at least two reasons. First, the signals we receive from the environments are often noisy. A signal in favor of potential change, for example a drop in COVID-19 cases, can either inform a true shift in regime or simply due to noisy fluctuations. Second, the signals we receive are subject to the volatility of the environment: while some environments are more prone to changes, others are not. In order to capture these two key features in regime-shift detection, we designed a novel fMRI task where subjects made probability judgments about regime shifts and where we manipulated the signal diagnosticity and transition probability. The former parameter captures the level of noise inherent in the signals, while the latter captures the volatility of the environment. We found that overreactions to regime shifts take place when participants received noisy signals (small signal diagnosticity) but when the environments were stable (small transition probability). By contrast, when the signals are more precise but the environments were unstable, participants tended to underreact to changes. These results suggest system neglect – people respond primarily to signals and secondarily to the system that generates the signals (Massey & Wu, 2005).

At the neurobiological level, we identified two building blocks for regime-shift estimation. The first building block is network-level computational specificity. We found that the neural computations for regime-shift estimation are supported by two distinct functional networks and each network has its own specified role. The vmPFC-striatum network is involved in computing and updating the probability estimates of regime shift. By contrast, a frontoparietal network including the dorsomedial prefrontal cortex, lateral prefrontal cortex (inferior frontal gyrus), and posterior parietal cortex (intraparietal sulcus), is involved in computing the strength of sensory evidence in favor of/against change and the base rate of change. These two computations are tightly linked: computing the probability estimate of change requires the decision maker's evaluation of the strength of sensory evidence and base rate. In summary, these two networks support the regime-shift estimation through performing distinct but intricately linked computations.

The second principle is network-level parameter selectivity. We found that these two networks showed dissociable patterns of parameter selectivity: while the frontoparietal network correlated with individual subjects' degree of neglecting the signal diagnosticity parameter, the vmPFC represented individuals' degree of neglecting the transition-probability parameter. Further, the brain regions within the frontoparietal network showed a remarkable consistency in coding the individual differences in signal-diagnosticity neglect only when the signals in favor of potential change appeared, whereas the vmPFC tracked transition-probability neglect regardless of whether the signals were in favor or against potential chance. These patterns of selectivity inspired a new behavioral analysis of the subjects' probability estimates data, which further confirmed what the neural data suggested. In summary, network-level computational specificity and parameter selectivity together are the two fundamental building blocks for system neglect.

Our work is closely related to the reversal-learning paradigm – the standard paradigm in neuroscience and psychology to study change detection. In a typical reversal-learning task, human or animal subjects choose between two options that differ in the value or probability of receiving a reward. Through reward feedback the participants gradually learn the reward contingencies associated with the options and have to update the contingencies when they switched in order to maximize rewards. While a switch in reward contingencies can be regarded as a kind of regime shift, there are 3 major differences between the reversal-learning paradigm and our regime-shift task. The first difference is about learning. In the reversal-learning paradigm, the subjects have to learn both the reward contingencies and the switches through experience. By contrast, in the regime-shift task, the subjects were explicitly informed about the makeup of different regimes and the transition probability. Therefore, participants do not need to learn about the different regimes and the transition probability through experience. The second difference is the kind of behavioral data collected. In our task, we asked the subjects to estimate the probability of change, whereas in the reversal-learning task, the subjects indicate their choice preferences. The third difference is on reward contingency. In the reversal-learning task, a change is specifically about change in reward contingencies, which is not the case in our task.

We believe that these major differences in task design led to three key insights into change detection from our study. The first insight is on over- and underreactions to change. At the behavioral level, we were able to identify situations that led to over-

and underreactions. At the theoretical level, we were able to provide a systematic account for these over- and underreactions in the system-neglect hypothesis. Finally, at the neurobiological level, we were able to quantify the degree to which individual subjects neglected the system parameters and use these behavioral measures to unravel the neural mechanisms that give rise to over- and underreactions to change.

The second insight is on the brain networks associated with change detection. In particular, we were able to clarify whether the neural systems involved in change detection in the reversal-learning tasks are contingent on whether rewards are involved. Since the reversal-learning tasks are about learning the reward contingencies and the change in reward contingencies, it would be more challenging to infer whether the neural implementations of change estimation are dissociable from reward estimation. Indeed, the brain regions shown to be involved in the reversal-learning tasks, the OFC, mPFC, striatum, and amygdala, were also found to be highly involved in reward-related learning and value-based decision making. In the current study, the subjects' task, which was to estimate the probability of change in regime, was not contingent on rewards. Therefore, the neural representations we found that were associated with change estimation, most notably the vmPFC and striatum for their involvement in the reversal-learning tasks, were dissociable from rewards, reward estimation, and reward-outcome contingency. This result therefore helps establish the involvement of vmPFC and striatum in change estimation independent of reward-guided learning and decision-making.

The third insight has to do with the impact of learning on change detection. Under the reversal-learning paradigm, it has been challenging to infer whether there exists a unique change-detection mechanism that is dissociable from reinforcement learning mechanisms. The way to make such inference is through theory, such as implementing a prior for state changes (Bartolo & Averbeck, 2020; Costa et al., 2015). Unlike the reversal-learning task, participants in our task did not have to learn about the different regimes through experience. Without having to consider the impact of reinforcement learning, our results help clarify the roles of change detection on choice behavior by suggesting that independent of learning, there exists a specialized change-detection mechanism in the brain that impacts decision making. Such mechanism involves the participation of the vmPFC-striatum network and the frontoparietal network, which partially overlap with the brain regions involved in reversal learning. However, it remains to be seen how learning interacts with change

detection. Future investigations can address this question by combining the key features of both the reversal-learning paradigm and regime-shift paradigm.

Our results are also closely related to the literature on the neural mechanisms for the evaluation and accumulation of sensory evidence in decision making (Gold & Shadlen, 2007; Mante et al., 2013; Philiastides et al., 2010; Roitman & Shadlen, 2002; Yates et al., 2017). The evaluation of sensory signals is central in the regime-shift task. In particular, the strength of evidence associated with a signal (blue or red ball) should depend on the signal diagnosticity. In a highly diagnostic environment, seeing a red ball should signal a strong possibility of being in the red regime, while seeing a blue ball should signal otherwise. By contrast, in a low diagnostic environment, seeing a red ball does not strongly indicate that the current regime is the red regime and seeing a blue ball also does not strongly indicate that the regime has shifted to the blue regime. Hence, the evaluation of sensory signals should reflect the interaction between the signals and the diagnosticity of the signals: a red signal (which we coded as 1 in our analysis) and a blue signal (which we coded as -1 in the analysis) should be weighted according to the level of signal diagnosticity.

We found that this key computation was implemented in a frontoparietal network commonly referred to as the frontoparietal control network (Buckner et al., 2013; Dosenbach et al., 2007; Seeley et al., 2007; Vincent et al., 2008; Yeo et al., 2011). This network was proposed to support adaptive control functions, including initiating control and providing flexibility to adjust the level of control through feedback (Dosenbach et al., 2007). The IPS and dlPFC, part of this network, have also been found to play a major role in the top-down control of attention (Corbetta & Shulman, 2002; Woldorff et al., 2004). In perceptual decision making, the IPS and dlPFC were also shown to represent the accumulation of sensory evidence that leads to the formation of a perceptual decision (Heekeren et al., 2004; Heekeren et al., 2006). Our findings—that activity in this network does not reflect just the sensory signals (red or blue balls) but how these signals should be interpreted through the lens of their diagnosticity—highlights the involvement of the frontoparietal control network in computing the strength of evidence through combining information about sensory signals and knowledge about the precision of those signals.

Our result on the intraparietal sulcus (IPS) being part of the brain network that represents diagnosticity-weighted sensory signals are consistent with previous studies showing that IPS is involved in accumulating sensory evidence over time (Gold &

Shadlen, 2007). There are three interesting aspects of our data that add to the current literature on evidence accumulation. First, IPS representations for sensory evidence need not be in the space of actions. Unlike previous studies showing that IPS represents sensory evidence for potential motor actions, we found that IPS represents the strength of evidence in favor of or against regime shifts (Fig. 5A). This result points to a more general role of the IPS in estimating the strength of sensory evidence. In fact, our result suggests that it depends on the task goal, which in the current study is to estimate whether a change has taken place. Second, although evidence accumulation is important and necessary for a wide array of cognitive functions, it is not a central requirement for the regime-shift task. Because the regime can change at any point in time, accumulating sensory evidence over time (counting the cumulated difference between the blue and red balls and weighted by the diagnosticity) and using it to estimate the likelihood of change is clearly suboptimal. In fact, this is only one of the possibilities. The regime can shift before the second observation, the third observation, and so on. To compute the likelihood ratio of regime shift, the decision maker needs to consider all these possibilities. In summary, here we showed that the IPS is critically involved in representing the strength of the current sensory evidence for regime shifts.

In the current study, the central opercular cortex—in addition to the vmPFC—is another brain region that represented the probability estimates of change. Like the vmPFC, activity in this region negatively correlated with the probability estimates of change. This finding is associated with previous findings on change detection using the oddball paradigm. Using the oddball paradigm, it was found that the central opercular cortex is involved in the detection of change, showing stronger activation in blocks containing only the standard stimulus than blocks containing both the standard and deviant stimulus (Hedge et al., 2015) and correlating with ERP P3 signals at the trial-level that reflected differences between standard and deviant stimuli (Warbrick et al., 2009). There are two implications here. First, our findings suggest that the central opercular cortex is not only involved in the detection of change—as revealed by the oddball tasks—but also is involved in the estimation of change when change is uncertain. Second, the central opercular cortex may be part of a common pathway for the detection of change across very different tasks whose common denominator is about change detection.

In summary, regime-shift estimation recruits two distinct brain networks that are defined by their unique computational roles. The vmPFC-striatum network represents the regime-shift probability estimates and is involved in updating one's beliefs about regime shift. By contrast, the frontoparietal network represents key variables necessary for producing regime-shift estimates. These two networks are associated with system neglect through their selective preferences for the system parameters: the vmPFC correlated with individuals' degree of neglecting the transition-probability parameter, while the frontoparietal network represented individuals' degree of neglecting the signal-diagnosticity parameter. Given that system neglect underlies a wide array of human judgments, our findings indicate that network-level computational specificity and parameter selectivity are two key building blocks that give rise to human judgment biases.

MATERIALS AND METHODS

We performed three fMRI experiments (90 subjects in total, 30 subjects for each experiment). Experiment 1 was the main experiment where we investigated the neurocomputational substrates for regime shifts. Experiments 2 and 3 were control experiments. Experiment 2 was an attempt to rule out brain activity that correlated with probability estimates but was not specifically about regime shifts. Experiment 3 was an attempt to rule out brain activity that correlated with entering numbers through button presses.

Subjects. All subject gave informed written consent to participate in the study. All study procedures were approved by the National Yang Ming Chiao Tung University Institutional Review Board. Ninety subjects participated in this study: Experiment 1: n = 30 subjects; 15 males; mean age: 22.9 years; age range: 20 to 29 yrs. Experiment 2: n = 30 subjects; 15 males; mean age: 23.3 years; age range, 20 to 30 years. Experiment 3: n = 30 subjects; 15 males; mean age: 23.7 years; age range: 20 to 34 years. The subjects were paid 300 New Taiwan dollar (TWD) for participating the behavioral session and 500 TWD for the fMRI session. Subjects received additional monetary bonus based on his or her performance on probability estimation in Experiments 1 and 2 (Experiment 1: an average of 209 and 212 TWD for the behavioral and fMRI session respectively; Experiment 2: an average of 223 and 206 TWD for the behavioral and fMRI session respectively). In Experiment 3, subjects received the bonus based on their performance on entering the correct number (an average of 243 TWD for the fMRI session).

Experiment 1

Procedure

Overview. The experiment consisted of two sessions—a behavioral session followed by an fMRI session—that took place on two consecutive days. The subjects performed the same task in both sessions. The goals of having the behavioral session were to train the subjects so that they became familiar with the task and to have enough trials—along with the fMRI session—so as to more reliably estimate the parameters of the computational models we tested (the power model and the system-

neglect model).

Regime-shift task. In this task, the environments the subjects were in were described as *regimes*. There were two possible regimes and at any point in time the regime can shift from one to another. The subjects' task was to judge whether the regime had shifted based on three sources of information: transition probability, signal diagnosticity, and signals. Prior to each trial, the subjects were given information about the transition probability and signal diagnosticity of the upcoming trial. The transition probability described how likely it is that the regime can shift from one to another. The signal diagnosticity described how different the two regimes are. The two regimes—red and blue—were represented by a red urn and a blue urn respectively, with each urn consisting of red and blue balls. The red urn had more red balls and the blue urn had more blue balls. The two urns always shared the same ratio of the dominant ball color to the dominated ball color. That is, the ratio of the red balls to the blue balls in the red urn was same as the ratio of the blue balls to the red balls in the blue urn. Signal diagnosticity was quantitatively defined by this ratio. For example, when the ratio was 9:1, signal diagnosticity was 9. Under this definition, larger signal diagnosticity indicated that the two regimes were more different from each other.

After information about the transition probability and signal diagnosticity were revealed, 10 sensory signals—red or ball balls shown on the computer screen—were sequentially presented to the subjects. Each signal was sampled with replacement from one of the two urns. We also referred to these signals as *observations*. By design, each trial always started at the red regime, but the regime can shift from the red to the blue regime at any point in time during a trial, including prior to the sampling of the first signal. In addition, also by design, the regime can shift only once in a trial. That is, once the regime changed from the red to the blue regime, signals would be sampled from the blue urn until the end of the trial. The subjects' task was to provide his or her estimate of the probability that current regime was the blue regime at each observation when a new signal was presented. Since the regime can only shift from the red to the blue, this probability estimate was equivalent to the probability estimate of regime shift.

Manipulations of transition probability and signal diagnosticity. We implemented a 3×3 factorial design where there were three possible transition probabilities, denoted as q where $q = [0.01, 0.5, 0.1]$ and three levels of signal diagnosticity, denoted as

d where $d = [1.5, 3, 9]$. The transition probability—the probability that the regime shifts from the red to the blue regime—was used to simulate the stability of the environment. Larger transition probabilities indicate less stable environments. The signal diagnosticity—the ratio of dominant balls to the dominated balls in the urns—was used to simulate the diagnosticity of the signals. For example, when $d = 9$, it indicates that the red balls are 9 times more than the blue balls in the red urn and that the blue balls are 9 times more than the red balls in the blue urn. In this case, the two regimes were highly different and hence the signals shown to the subjects should be highly diagnostic of the regime the subjects were currently in.

Session 1: behavioral session

A pre-test block followed by the main task (8 blocks of trials) were implemented in the behavioral session. We implemented the pre-test block to make sure the subjects understood the experimental instructions and to train them to become familiar with the task, especially the time limit in entering probability estimates (see Trial sequence below for details on the pre-test block). A 3 (transition probability) by 3 (signal diagnosticity) factorial design was implemented, resulting in a total of 9 experimental conditions. Each block consisted of 9 trials (one for each condition, randomized in order) and each trial consisted of 10 observations or equivalently, 10 sequentially presented signals. After the pre-test block, subjects performed the main task that consisted of 8 blocks of trials. The behavioral session took approximately 70 minutes to complete.

Trial sequence. At the beginning of each trial, the subjects were shown information about the transition probability and signal diagnosticity (3s) (Fig. 1A). This was followed by the sequential presentation of 10 observations. At each observation, a signal—a red or blue dot sampled from the current regime was shown. Subjects' task was to estimate the probability that the current regime was the blue regime within 4s. The subjects indicated the probability estimate through two button presses. During the experiment, the subjects placed his or her 10 fingers on a 10-button keypad. Each finger was associated with a single button that corresponded to a unique integer value from 0 to 9. To enter the probability estimate, the subjects had to first press the number corresponding to the tens and second the number corresponding to the ones. For example, if the probability estimate was 95%, the subjects first had to press the

“9” button and second the “5” button. Once the subjects entered the probability estimate, she or he was not allowed to change it. After providing the probability estimate, they were given a brief feedback (0.5s) on the number they just entered. If they failed to indicate probability estimate within the time limit (4s), a “too slow” message would be shown. At the end of each trial, the subjects received feedback (2s) on the amount of monetary bonus earned in the trial (2s) and information about whether the regime shifted during the trial. If the regime was shifted, the signal that was drawn right after the shift took place would be highlighted in white. This was followed by a variable inter-trial interval (ITI, 1s to 5s in steps of 1s drawn from a discrete uniform distribution).

We implemented a pre-test block at the beginning of the behavioral so as to train the subjects to enter the probability estimate within the time limit (4s). In the pre-test block, we started with a lenient time limit and gradually decreased it. The time limit for the first three trials was 20s, 10s from trial number 4 to 6, and 4s from trial number 7 to 9. Recall that in each trial, the subjects encountered 10 sequentially presented observations (red and blue balls) and had to provide probability estimate at each observation. The subjects therefore entered 30 probability estimates under each of these three time limits—from 20s, 10s, to 4s. After the pre-test block, all the subjects were able to enter the probability estimates within 4s.

Session 2: fMRI session

The fMRI session consisted of 3 blocks (9 trials in each block, with each trial consisting of 10 sequentially presented signals). The task was identical to the behavioral session (except with varying inter-stimulus interval for the purpose of fMRI analysis) and took approximately 60 minutes to complete. The trial sequence was identical to the behavioral session with a few exceptions. First, each new signal was presented for 4s regardless of when subjects make a response. Second, we added a variable inter-stimulus interval (ISI, 1s to 5s in steps of 1 drawn from a uniform distribution) between two successive signals. We also made the range of ITI to be slightly larger (1s to 7s drawn from a discrete uniform distribution between in steps of 1s) than the behavioral session. The design of variable ISIs and ITIs was to allow better dissociations between events, i.e. between different sensory signals presented during a trial, and between trials for fMRI analysis.

Monetary bonus

To incentivize the subjects to perform well in this experiment, they received monetary bonus based on his or her probability estimates. The bonus rule was designed so that the subjects who gave more accurate estimates would earn more bonus

$$Bonus(t) = \$30 \times \left(0.1 - 0.2 \times \left(P_t^e - B_t\right)^2\right)$$

where P_t^e is the probability estimate that the current regime was blue at the *t*-th signal in a trial and B_t is the regime at *t* ($B_t = 1$ for the blue regime and $B_t = 0$ for the red regime). For each probability estimate, the bonus therefore ranged from winning $3 to losing $3 TWD. For example, if the subject gave a 99% probability estimate that the current regime was blue and the current regime was indeed the blue regime, she would receive a bonus close to 3 TWD. By contrast, if the subjects gave a 1% probability estimate that the current regime was blue but the current regime was the red regime, she would receive a penalty close to 3 TWD. With 10 probability estimates given in each trial, the subjects can therefore receive a bonus up to 30 TWD or a penalty up to 30 TWD in a trial. The subjects did not receive feedback on bonus after each probability estimate. Instead, at the end of each trial, the subjects received information about the total amount won or lost in that trial. The final total bonus was realized by randomly selecting 10 trials at the end of the experiment.

Computational models for regime shift

We examined three computational models for regime shift: the Bayesian model, the power model, and the system-neglect model (Massey & Wu, 2005). The Bayesian model was parameter-free and was used to compare with the subjects' probability estimates of regime shift. The power model and the system-neglect model were quasi-Bayesian models—parameterized versions of the Bayesian model—that were fit to the subjects' probability-estimate data. The parameter estimates of the system-neglect model were further used in the fMRI analysis so as to identify neural representations for over- and underreactions to change.

Bayesian model

Here we describe the Bayesian posterior odds of shifting to the blue regime given the observation history H_t (Edwards, 1968; Massey & Wu, 2005)

$$\frac{P_t^{Bayes}}{1-P_t^{Bayes}} = \frac{\Pr\left(B_t \middle| H_t\right)}{\Pr\left(R_t \middle| H_t\right)} = \frac{1-\left(1-q\right)^t}{\left(1-q\right)^t} \sum_{j=1}^{t} \frac{q\left(1-q\right)^{j-1}}{1-\left(1-q\right)^t} d^{\,t+1-j-2\sum_{k=j}^{t} r_k} . \qquad (1)$$

P_t^{Bayes} is the posterior probability that the regime has shifted to the blue regime at the *t*-th observation $\Pr\left(B_t \middle| H_t\right)$ where H_t denotes the sequence of observation history form r_1 to r_t. Here r_t donates the *t*-th observation: $r_t = 1$ when the signal at *t* is red, $r_t = 0$ when the signal at *t* is blue. The transition probability and signal diagnosticity are denoted by *q* and *d* respectively.

The posterior odds are the product of the prior odds and the likelihood ratio. The prior odds, $\frac{1-\left(1-q\right)^t}{\left(1-q\right)^t}$, indicates that given the transition probability *q*, the probability that the regime has shifted at time *t*, $1-\left(1-q\right)^t$, relative to the probability of no change in regime, $\left(1-q\right)^t$. The likelihood ratio, $\sum_{j=1}^{t} \frac{q\left(1-q\right)^{j-1}}{1-\left(1-q\right)^t} d^{\,t+1-j-2\sum_{k=j}^{t} r_k}$, indicates the probability of observing the signals presented thus far (H_t: observation history) given that the regime has shifted relative to the probability of observing the signals given that the regime has not shifted. This requires considering all the possibilities on the timing of shift, i.e. the likelihood ratio that the regime was shifted at *t=j*, $d^{\,t+1-j-2\sum_{k=j}^{t} r_k}$, weighted by its odds $\frac{q\left(1-q\right)^{j-1}}{1-\left(1-q\right)^t}$. Since these possibilities are disjoint events, the likelihood ratio that the regime has shifted is simply the weighted sum of all the likelihood ratios associated with these disjoint possibilities.

Index of overreaction to change

To quantify under- and overreactions to change, we derived an Index of Overreaction (*IO*). In short, this index reflects the degree to which the subjects overreacted or underreacted to change such that an index value greater than 0 indicates overreaction and an index value smaller than 0 suggests underreaction. To compute *IO*, we compared the change in the subjects' actual probability estimates between two successive observations ($\Delta P_t^e = P_t^e - P_{t-1}^e$) with the ideal change in probability estimates according to the ideal Bayesian model ($\Delta P_t^b = P_t^b - P_{t-1}^b$). Here we use P_t^e to denote the subject's probability estimate at the *t*-th observation and P_t^b to denote the ideal Bayesian probability estimate. We computed *IO* ($IO = \Delta P_t^e - \Delta P_t^b$) separately for each subject and for each condition (a combination of transition probability and signal diagnosticity). Overreaction is defined when the actual change in probability estimates is greater than the ideal change in probability estimates ($\Delta P_t^e > \Delta P_t^b$). Therefore, the *IO* would be greater than 0 when the subjects overreacted. By contrast, underreaction is defined when the actual change is smaller than the ideal change in probability estimate ($\Delta P_t^e < \Delta P_t^b$). Hence, *IO* would be smaller than 0 when the subjects underreacted. When there is no difference between the two, the subjects' responses were ideal and therefore she or he neither overreacted nor underreacted to change.

Parameter estimation

We fit two quasi-Bayesian models—the power model and the system-neglect model. The power model estimated the subjects' sensitivity to transition probability and signal diagnosticity. Two parameters, α and β, were added to Eq. (1) to capture the sensitivity to transition probability and signal diagnosticity respectively such that

$$\frac{P_t^e}{1-P_t^e} = \frac{\Pr\left(B_t \middle| H_t\right)}{\Pr\left(R_t \middle| H_t\right)} = \frac{1-\left(1-\alpha q\right)^t}{\left(1-\alpha q\right)^t} \sum_{j=1}^{t} \frac{q\left(1-q\right)^{j-1}}{1-\left(1-q\right)^t} d^{\beta\left(t+1-j-2\sum_{k=j}^{t} r_k\right)} \tag{2}$$

where P_t^e is the probability estimate that regime has changed to the blue regime at observation number *t* predicted by the power model.

In contrast to the power model that estimated the overall sensitivity – across levels – to transition probability and signal diagnosticity, the system-neglect model separately estimated the sensitivity to each level of transition probability and signal diagnosticity. This was implemented by setting dummy variables for each level of

transition probability and signal diagnosticity in Eq. (2)

$$\alpha = \alpha_1 Q_1 + \alpha_2 Q_2 + \alpha_3 Q_3 \quad \text{and} \quad \beta = \beta_1 D_1 + \beta_2 D_2 + \beta_3 D_3$$

where Q_m is the dummy variable for transition probability under q_m and D_n is the dummy variable for diagnosticity under d_n. α_m and β_n therefore respectively reflect the sensitivity to different levels of transition probability and signal diagnosticity. The system-neglect model is an extension of the power model, as it allows α_m and β_n to differ between levels.

Experiment 2

The procedure of Experiment 2 was identical to Experiment 1, except that there was no regime shift in this experiment. In other words, we only manipulated the signal diagnosticity in this experiment. The regime that the sensory signals were drawn from (red or blue urn) was randomly determined such that in half of the trials the regime was red and the other half the regime was blue. The order of the regimes across trials was pseudo randomized for each subject separately. Identical to Experiment 1, the subjects in Experiment 2 were instructed to estimate the probability that regime was the blue urn at the presentation of each new signal. Therefore, in both Experiments 1 and 2, the subjects estimated the probability that the current regime was the blue regime. However, it was only in Experiment 1 that the probability estimates conveyed information about the subjects' belief about change (whether the regime had shifted).

Bayesian model

The Bayesian posterior odds of the blue regime at the *t*-th observation given the observation history H_t were calculated by following equation

$$\frac{P_t^{Bayes}}{1-P_t^{Bayes}} = \frac{\Pr(B|H_t)}{\Pr(R|H_t)} = \frac{\Pr(B)}{\Pr(R)} \times \frac{\Pr(H_t|B)}{\Pr(H_t|R)} \tag{3}$$

where $\frac{\Pr(B)}{\Pr(R)}$ is the prior odds and $\frac{\Pr(H_t|B)}{\Pr(H_t|R)}$ is the likelihood ratio. Given that the probability of being in the blue regime and being in the red regime were equal

$\Pr(B) = \Pr(R) = 0.5$, Eq. (3) can be rewritten as

$$\frac{P_t^{Bayes}}{1-P_t^{Bayes}} = \frac{\Pr(B|H_t)}{\Pr(R|H_t)} = \frac{0.5}{0.5} \times \frac{\Pr(H_t|B)}{\Pr(H_t|R)} = \frac{\Pr(H_t|B)}{\Pr(H_t|R)}. \tag{4}$$

The likelihood ratio is computed according to the following equation

$$\frac{\Pr(H_t|B)}{\Pr(H_t|R)} = d^{t-2\sum_{k=1}^{t} r_k} \tag{5}$$

where d represents signal diagnosticity. The exponent of d captures the difference between the number of the blue balls and red balls from the first to the t-th observation. For example, suppose that at the 5th observation there are 4 red balls and 1 blue ball. Then $d^{t-2\sum_{k=1}^{t} r_k}$ would be $d^{5-2\times 4} = d^{-3}$ where the exponent is the number of blue balls minus the number of red balls.

Parameter estimation

Similar to Experiment 1, we fit two models, the power model and the system-neglect model. The power model consisted of a single parameter β to capture the overall sensitivity to signal diagnosticity (across different levels)

$$\frac{P_t^b}{1-P_t^b} = \frac{\Pr(B_t|H_t)}{\Pr(R_t|H_t)} = d^{\beta\left(t-2\sum_{k=1}^{t} r_k\right)} \tag{4}$$

The system-neglect model is an extension of the power model. It separately estimated β for each level of signal diagnosticity

$$\beta = \beta_1 D_1 + \beta_2 D_2 + \beta_3 D_3$$

where D_n is the dummy variable for diagnosticity under d_n.

Experiment 3

We referred to Experiment 3 as the motor-equivalent task of Experiments 1 and 2. The

primary goal of this experiment was to rule out the motor confounds for probability estimates in Experiment 1. We were aware that brain regions whose activity correlated with probability estimates in Experiment 1 can simply reflect the entering of numbers through button presses and had nothing to do with estimating the probability of change. Therefore, to establish the evidence for the neural representations of probability estimates, we needed to rule out the motor confounds. The motor-equivalent task shared many of the physical and motor aspects of the tasks in Experiments 1 and 2. First, the task structure was identical. In the motor-equivalent task, each trial contained ten rounds. In each round, a hollow dot with no color information was shown to indicate the number of this round. A random number from 0 to 99 was presented at the center of screen. Subjects had to enter the indicated number with two successive button presses within 4 seconds. After this button-press stage there were a feedback on the number they just entered. If they correctly entered the indicated number, the feedback was shown in white. The feedback would change to yellow if the entered number was incorrect. The reward was $3 for each correct answer and -$3 for incorrect answer. The accumulated reward outcome for each trial was revealed at the end of the trial.

fMRI data acquisition. All the imaging parameters, including the EPI sequence and MPRAGE sequence, remained the same throughout the three experiments. For Experiments 1 and 2, the subjects completed the task in a 3T Siemens MRI scanner (MAGNETOM Trio) equipped with a 32-channel head array coil. Experiment 3 was collected at a later date after the same scanner went through a major upgrade (from Trio to the Prisma system) where a 64-channel head array coil was used. Each subject completed three functional runs. Before each run, a localizer scan was implemented for slice positioning. For each run, T2*-weighted functional images were collected using an EPI sequence (TR=2000ms, TE=30ms, 33 oblique slices acquired in ascending interleaved order, 3.4×3.4×3.4 mm isotropic voxel, 64×64 matrix in 220 mm field of view, flip angle 90°). To reduce signal loss in the ventromedial prefrontal cortex and orbitofrontal cortex, the sagittal axis was tilted clockwise up to 30°. Each run consisted of 9 trials and a total of 374 images. After the functional scans, T1-weighted structural images were collected (MPRAGE sequence with TR=2530ms, TE=3.03ms, flip angle=7°, 192 sagittal slices, 1×1×1 mm isotropic voxel, 224×256 matrix in a 256-mm field of view). For each subject, a field map image was also

acquired for the purpose of estimating and partially compensating for geometric distortion of the EPI image so as to improve registration performance with the T1-weighted images.

fMRI preprocessing. The imaging data were preprocessed with FMRIB's software Library (FSL version 6.0). First, for motion correction, MCFLIRT was used to remove the effect of head motion during each run. Second, FUGUE (FMRIB's Utility for Geometric Unwarping of EPIs) was used to estimate and partially compensate for geometric distortion of the EPI images using field map images collected for the subject. Third, spatial smoothing was applied with a Gaussian kernel with FWHM=6mm. Fourth, a high-pass temporal filtering was applied using Gaussian-weighted least square straight-line fitting with $\sigma = 50s$. Fifth, registration was performed in a two-step procedure, with the field map used to improve the performance of registration. First, EPI images were registered to the high-resolution brain T1-weighted structural image (non-brain structures were removed via FSL's BET (Brain Extraction Tool). Second, the transformation matrix (12-parameter affine transformation) from the T1-weighted image to the Montreal Neurological Institute (MNI) template brain was estimated using FLIRT (FMRIB's Linear Image Registration Tool), followed by nonlinear registration using FNIRT (FMRIB's Non-linear Image Registration Tool) with a 10mm warp resolution. This two-step procedure allowed for transforming the EPI images to the standard MNI template brain.

General Linear Models of BOLD signals

All GLM analyses were carried out in the following steps (Beckmann et al., 2003). First, BOLD time series were pre-whitened with local autocorrelation correction. A first-level FEAT analysis was carried out for each run of each subject. Second, a second-level (subject-level) fixed-effect (FE) analysis was carried out for each subject that combined the first-level FEAT results from different runs using the summary statistics approach. Finally, a third-level (group-level) mixed-effect (ME) analysis using FSL's FLAME module (FMRIB's Local Analysis of Mixed Effects) was carried out across subjects by taking the FE results from the previous level and treating subjects as a random effect (Woolrich et al., 2004). All reported whole-brain results

were corrected for multiple comparisons. We first identified clusters of activation by defining a cluster-forming threshold of the z statistic ($z>3.1$ or equivalently $p<0.001$) (Eklund et al., 2016; Woo et al., 2014).Then, a family-wise error corrected p-value of each cluster based on its size was estimated using Gaussian random field theory (Worsley et al., 1992). In addition, we performed nonparametric permutation test using the randomize function in FSL (threshold-free cluster enhancement or TFCE option; (Smith & Nichols, 2009) on all the contrasts reported.

GLM-1. This model was used for Fig 3. The model served two purposes. First, we used it to examine neural representations for probability estimates (Fig. 3B). Second, we used this model to compare results from the three experiments (Experiments 1 to 3) (Fig. 3C-E). We implemented the following regressors. At the time of each signal presentation, we implemented the following regressors: (R1) an indicator regressor with length equal to the subject's RT, (R2) R1 multiplied by the subject's probability estimate $\hat{P}$, (R3) R1 multiplied by the degree of certainty in probability estimate $\left|\hat{P}-0.5\right|$, and (R4) R1 multiplied by the observation number (from 1 to 10). Both positive and negative contrasts of R2, R3, and R4 were set up to identify activity that either positively or negatively correlate with probability estimates (R2), degree of certainty (R3), and observation number (R4). At the end of each trial (after the subjects saw all the 10 signals), we showed how much monetary bonus the subject won in that trial. We implemented an indicator regressor (R5) and a parametric regressor for the subject's winning (R6). Finally, we implemented an indicator regressor (length equal to 4s) for no-response observations. These corresponded to the observation(s) where the subject did not indicate the probability estimate within the time limit (4s).

GLM-2. This model was used for Figs. 4 and 5. In Fig. 4, the result on the updating of beliefs about change (orange clusters) was based on R5 and the result on the probability estimates (blue clusters) was based on R2 in this model. In Fig. 5, the result on the interaction between signal and signal diagnosticity was based on R11, and the result on the interaction between signal and transition probability was based on R10. We implemented the following regressors. At the time of signal presentation,

the model was identical to GLM-1 (R1 to R4) except with the addition of the following regressors: (R5) R1 multiplied by difference in the subject's probability estimate between two successive observations, which captured the updating of the subjects' belief about change, (R6) R1 multiplied by transition probability, (R7) R1 multiplied by the natural logarithm of signal diagnosticity, (R8) R1 multiplied by the current signal (1 for blue ball, -1 for red ball), (R9) the interaction R7$\times$R8 (interaction between transition probability and signal diagnosticity), (R10) the interaction R7$\times$R9 (interaction between transition probability and signal), (R11) the interaction R8$\times$R9 (interaction between signal diagnosticity and signal). The purpose of having R6 to R11 was to rule out the possibility of attributing the updating of beliefs about change to these regressors, which affected the updating of beliefs and were therefore correlated with the updating of beliefs. Finally, at the end of each trial (after the subjects saw all the 10 signals), we implemented (R12) an indicator regressor and (R13) subject's current-trial monetary bonus. R12 and R13 were identical to the R5 and R6 in GLM-1. Finally, we implemented an indicator regressor (length equal to 4s) for no-response observations. These corresponded to the observation(s) where the subject did not indicate the probability estimate within the time limit (4s).

GLM-3. This model was the basis of results shown in Fig. 6. We set up two sets of regressors, one set for when the blue signal (signal for potential change) appeared and the other for when the red signal (signal for no change) appeared. For each set, at the time of signal presentation, we implemented 9 indicator regressors, each for a combination of transition probability (3 levels) and signal diagnosticity (3 levels). Based on these 9 regressors, we set up a linear-increasing contrast separately for signal diagnosticity and transition probability. At the subject level (second level), the parameter estimate of these contrasts reflects individual subjects' sensitivity to signal diagnosticity and transition probability were extracted from a given ROI, and was used to correlate with individual subjects' behavioral sensitivity to signal diagnosticity and transition probability. The ROIs used were vmPFC, ventral striatum, dmPFC, bilateral IFG, and bilateral IPS. These ROIs were identified by results from GLM 1 and 2 and were constructed in a statistically independent manner using leave-one-subject-out method. See Independent region-of-interest (ROI) analysis in the section below. Same as in the previous two GLMs, at the end of each trial when

feedback on the current-trial monetary bonus was revealed, we implemented an indicator regressor and a parametric regressor for the monetary bonus. Finally, we implemented an indicator regressor (length equal to 4s) for no-response observations. These corresponded to the observation(s) where the subject did not indicate the probability estimate within the time limit (4s).

Psychophysiologic interaction (PPI) analysis. The result of this analysis was presented in Figure 7. To investigate whether the functional connectivity between the vmPFC and the frontoparietal network would differ in a signal-dependent fashion, we set up the following PPI analysis. We used the vmPFC ROI from Bartra et al. (2013) as the seed region, extracted and deconvolved its BOLD timeseries data separately for each run of each subject (Gitelman et al., 2003). The deconvolved BOLD data are implemented as a regressor in this GLM (the physiological regressor). Two regressors, one for the presentation of the blue signals and the other for the red signals, were also implemented (psychological regresssors). Two interaction regressors, one for the interaction between the vmPFC timeseries and the blue-signal regressor and the other for the interaction between the vmPFC timeseries and the red-signal regressor, were also implemented. In addition, separately for the blue-signal and red-signal observations, subject's probability estimates and degree of certainty were implemented as regressors. Same as in the previous two GLMs, at the end of each trial when feedback on the current-trial monetary bonus was revealed, we implemented an indicator regressor and a parametric regressor for the monetary bonus. Finally, we implemented an indicator regressor (length equal to 4s) for no-response observations. These corresponded to the observation(s) where the subject did not indicate the probability estimate within the time limit (4s).

Independent regions-of-interest (ROIs) analysis. We performed two kinds of independent ROI analysis—leave-one-subject-out (LOSO) method and functional masks based on previous meta-analysis paper. We used the functional masks in vmPFC from Bartra et al. (2013). For LOSO, based on results from the whole-brain analysis, we created independent and unbiased ROIs using the leave-one-subject-out (LOSO) method (Litt et al., 2011; Ting et al., 2015). The LOSO method was used to analyze probability estimates, and representations for transition probability and signal

diagnosticity described above. For each subject separately, we performed the analysis in the following steps. First, we identified the significant cluster in a brain region (e.g., dmPFC) that correlated with a contrast of interest (e.g., probability estimates) using all other subjects' data. We referred to this as the LOSO ROI. Second, we extracted the mean beta value (regression coefficient) within the LOSO ROI from the subject and used it for further statistical analysis. Note that the LOSO ROI tended to be different spatially between subjects. To give an idea of these differences and the spatial distribution of these ROIs, in Figs. 5 and 6 where the LOSO analysis was performed, we showed both the voxels that were part of the LOSO ROI of all the subjects in one color and the voxels that were part of at least one LOSO ROI in another color.

ACKNOWLEDGMENTS

This work was supported by the National Science and Technology Council (NSTC) in Taiwan (Grants 108-2410-H-010-012-MY3, 110-2410-H-A49A-504 -MY3 to S.-W.W.) and by the Brain Research Center, National Yang Ming Chiao Tung University from The Featured Areas Research Center Program within the framework of the Higher Education Sprout Project by the Ministry of Education (MOE) in Taiwan. We acknowledge magnetic resonance imaging support from National Yang Ming Chiao Tung University, Taiwan, which is in part supported by the Ministry of Education plan for the top University.

References

Bartolo, R., & Averbeck, B. B. (2020). Prefrontal Cortex Predicts State Switches during Reversal Learning. *Neuron*, *106*(6), 1044-1054 e1044. https://doi.org/10.1016/j.neuron.2020.03.024

Bartra, O., McGuire, J. T., & Kable, J. W. (2013). The valuation system: a coordinate-based meta-analysis of BOLD fMRI experiments examining neural correlates of subjective value. *Neuroimage*, *76*, 412-427.

Beck, D. M., Muggleton, N., Walsh, V., & Lavie, N. (2006). Right parietal cortex plays a critical role in change blindness. *Cereb Cortex*, *16*(5), 712-717. https://doi.org/10.1093/cercor/bhj017

Beck, D. M., Rees, G., Frith, C. D., & Lavie, N. (2001). Neural correlates of change detection and change blindness. *Nat Neurosci*, *4*(6), 645-650. https://doi.org/10.1038/88477

Beckmann, C. F., Jenkinson, M., & Smith, S. M. (2003). General multilevel linear modeling for group analysis in FMRI. *NeuroImage*, *20*(2), 1052-1063. http://www.sciencedirect.com/science/article/pii/S105381190300435X

Behrens, T. E., Woolrich, M. W., Walton, M. E., & Rushworth, M. F. (2007). Learning the value of information in an uncertain world. *Nat Neurosci*, *10*(9), 1214-1221. https://doi.org/10.1038/nn1954

Boorman, E. D., Rajendran, V. G., O'Reilly, J. X., & Behrens, T. E. (2016). Two Anatomically and Computationally Distinct Learning Signals Predict Changes to Stimulus-Outcome Associations in Hippocampus. *Neuron*, *89*(6), 1343-1354. https://doi.org/10.1016/j.neuron.2016.02.014

Boorman, E. D., Rushworth, M. F., & Behrens, T. E. (2013). Ventromedial prefrontal and anterior cingulate cortex adopt choice and default reference frames during sequential multi-alternative choice. *J Neurosci*, *33*(6), 2242-2253. https://doi.org/10.1523/JNEUROSCI.3022-12.2013

Buckner, R. L., Krienen, F. M., & Yeo, B. T. (2013). Opportunities and limitations of intrinsic functional connectivity MRI. *Nat Neurosci*, *16*(7), 832-837. https://doi.org/10.1038/nn.3423

Corbetta, M., & Shulman, G. L. (2002). Control of goal-directed and stimulus-driven attention in the brain. *Nat Rev Neurosci*, *3*(3), 201-215. https://doi.org/10.1038/nrn755

Costa, V. D., Tran, V. L., Turchi, J., & Averbeck, B. B. (2015). Reversal learning and dopamine: a bayesian perspective. *J Neurosci*, *35*(6), 2407-2416. https://doi.org/10.1523/JNEUROSCI.1989-14.2015

Dosenbach, N. U., Fair, D. A., Miezin, F. M., Cohen, A. L., Wenger, K. K., Dosenbach, R. A., Fox, M. D., Snyder, A. Z., Vincent, J. L., Raichle, M. E., Schlaggar, B. L., & Petersen, S. E. (2007). Distinct brain networks for adaptive and stable task control in humans. *Proc Natl Acad Sci U S A*, *104*(26), 11073-11078. https://doi.org/10.1073/pnas.0704320104

Edwards, W. (1968). Conservatism in human information processing. *Formal representation of human judgment*.

Eklund, A., Nichols, T. E., & Knutsson, H. (2016). Cluster failure: Why fMRI inferences for spatial extent have inflated false-positive rates. *Proceedings of the National Academy of Sciences*, *113*(28), 7900-7905.

Gitelman, D. R., Penny, W. D., Ashburner, J., & Friston, K. J. (2003). Modeling regional and psychophysiologic interactions in fMRI: the importance of hemodynamic deconvolution. *NeuroImage*, *19*(1), 200-207.

Gold, J. I., & Shadlen, M. N. (2007). The neural basis of decision making. *Annu. Rev. Neurosci.*, *30*, 535-574.

Gutteling, T. P., Park, S. Y., Kenemans, J. L., & Neggers, S. F. (2013). TMS of the anterior intraparietal area selectively modulates orientation change detection during action preparation. *J Neurophysiol*, *110*(1), 33-41. https://doi.org/10.1152/jn.00622.2012

Hedge, C., Stothart, G., Todd Jones, J., Rojas Frias, P., Magee, K. L., & Brooks, J. C. (2015). A frontal attention mechanism in the visual mismatch negativity. *Behav Brain Res*, *293*, 173-181. https://doi.org/10.1016/j.bbr.2015.07.022

Heekeren, H. R., Marrett, S., Bandettini, P. A., & Ungerleider, L. G. (2004). A general mechanism for perceptual decision-making in the human brain. *Nature*, *431*(7010), 859-862. https://doi.org/10.1038/nature02966

Heekeren, H. R., Marrett, S., Ruff, D. A., Bandettini, P. A., & Ungerleider, L. G. (2006). Involvement of human left dorsolateral prefrontal cortex in perceptual decision making is independent of response modality. *Proc Natl Acad Sci U S A*, *103*(26), 10023-10028. https://doi.org/10.1073/pnas.0603949103

Huettel, S. A., Guzeldere, G., & McCarthy, G. (2001). Dissociating the neural mechanisms of visual attention in change detection using functional MRI. *J*

Cogn Neurosci, *13*(7), 1006-1018. https://doi.org/10.1162/089892901753165908

Izquierdo, A., Brigman, J. L., Radke, A. K., Rudebeck, P. H., & Holmes, A. (2017). The neural basis of reversal learning: An updated perspective. *Neuroscience*, *345*, 12-26. https://doi.org/10.1016/j.neuroscience.2016.03.021

Jocham, G., Brodersen, K. H., Constantinescu, A. O., Kahn, M. C., Ianni, A. M., Walton, M. E., Rushworth, M. F., & Behrens, T. E. (2016). Reward-guided learning with and without causal attribution. *Neuron*, *90*(1), 177-190.

Kremer, M., Moritz, B., & Siemsen, E. (2011). Demand Forecasting Behavior: System Neglect and Change Detection. *Management Science*, *57*(10), 1827-1843. https://doi.org/10.1287/mnsc.1110.1382

Litt, A., Plassmann, H., Shiv, B., & Rangel, A. (2011). Dissociating Valuation and Saliency Signals during Decision-Making. *Cerebral Cortex*, *21*(1), 95-102. http://cercor.oxfordjournals.org/content/21/1/95.abstract

Mante, V., Sussillo, D., Shenoy, K. V., & Newsome, W. T. (2013). Context-dependent computation by recurrent dynamics in prefrontal cortex. *Nature*, *503*(7474), 78-84.

Massey, C., & Wu, G. (2005). Detecting regime shifts: The causes of under-and overreaction. *Management Science*, *51*(6), 932-947.

Naatanen, R., Teder, W., Alho, K., & Lavikainen, J. (1992). Auditory attention and selective input modulation: a topographical ERP study. *Neuroreport*, *3*(6), 493-496. https://doi.org/10.1097/00001756-199206000-00009

Pessoa, L., & Ungerleider, L. G. (2004). Neural correlates of change detection and change blindness in a working memory task. *Cereb Cortex*, *14*(5), 511-520. https://doi.org/10.1093/cercor/bhh013

Philiastides, M. G., Biele, G., & Heekeren, H. R. (2010). A mechanistic account of value computation in the human brain. *Proceedings of the National Academy of Sciences*, *107*(20), 9430-9435.

Reddy, L., Quiroga, R. Q., Wilken, P., Koch, C., & Fried, I. (2006). A single-neuron correlate of change detection and change blindness in the human medial temporal lobe. *Curr Biol*, *16*(20), 2066-2072. https://doi.org/10.1016/j.cub.2006.08.064

Rensink, R. A. (2002). Change detection. *Annu Rev Psychol*, *53*(1), 245-277. https://doi.org/10.1146/annurev.psych.53.100901.135125

Roitman, J. D., & Shadlen, M. N. (2002). Response of neurons in the lateral intraparietal area during a combined visual discrimination reaction time task. *Journal of Neuroscience*, *22*(21), 9475-9489.

Sabri, M., Radnovich, A. J., Li, T. Q., & Kareken, D. A. (2005). Neural correlates of olfactory change detection. *Neuroimage*, *25*(3), 969-974. https://doi.org/10.1016/j.neuroimage.2004.12.033

Sanders, N. R., & Manrodt, K. B. (2003). Forecasting Software in Practice: Use, Satisfaction, and Performance. *Interfaces*, *33*(5), 90-93. https://doi.org/10.1287/inte.33.5.90.19251

Seeley, W. W., Menon, V., Schatzberg, A. F., Keller, J., Glover, G. H., Kenna, H., Reiss, A. L., & Greicius, M. D. (2007). Dissociable intrinsic connectivity networks for salience processing and executive control. *J Neurosci*, *27*(9), 2349-2356. https://doi.org/10.1523/JNEUROSCI.5587-06.2007

Seifert, M., Ulu, C., & Guha, S. (2023). Decision Making Under Impending Regime Shifts. *Management Science*. https://doi.org/10.1287/mnsc.2022.4661

Smith, S. M., & Nichols, T. E. (2009). Threshold-free cluster enhancement: addressing problems of smoothing, threshold dependence and localisation in cluster inference. *NeuroImage*, *44*(1), 83-98.

Soltani, A., & Izquierdo, A. (2019). Adaptive learning under expected and unexpected uncertainty. *Nat Rev Neurosci*, *20*(10), 635-644. https://doi.org/10.1038/s41583-019-0180-y

Takahashi, Y. K., Roesch, M. R., Wilson, R. C., Toreson, K., O'Donnell, P., Niv, Y., & Schoenbaum, G. (2011). Expectancy-related changes in firing of dopamine neurons depend on orbitofrontal cortex. *Nat Neurosci*, *14*(12), 1590-1597. https://doi.org/10.1038/nn.2957

Ting, C.-C., Yu, C.-C., Maloney, L. T., & Wu, S.-W. (2015). Neural Mechanisms for Integrating Prior Knowledge and Likelihood in Value-Based Probabilistic Inference. *The Journal of Neuroscience*, *35*(4), 1792-1805.

Vincent, J. L., Kahn, I., Snyder, A. Z., Raichle, M. E., & Buckner, R. L. (2008). Evidence for a frontoparietal control system revealed by intrinsic functional connectivity. *J Neurophysiol*, *100*(6), 3328-3342. https://doi.org/10.1152/jn.90355.2008

Walton, M. E., Behrens, T. E., Buckley, M. J., Rudebeck, P. H., & Rushworth, M. F. (2010). Separable learning systems in the macaque brain and the role of

orbitofrontal cortex in contingent learning. *Neuron*, *65*(6), 927-939. https://doi.org/10.1016/j.neuron.2010.02.027

Wang, F., Schoenbaum, G., & Kahnt, T. (2020). Interactions between human orbitofrontal cortex and hippocampus support model-based inference. *PLoS Biol*, *18*(1), e3000578. https://doi.org/10.1371/journal.pbio.3000578

Warbrick, T., Mobascher, A., Brinkmeyer, J., Musso, F., Richter, N., Stoecker, T., Fink, G. R., Shah, N. J., & Winterer, G. (2009). Single-trial P3 amplitude and latency informed event-related fMRI models yield different BOLD response patterns to a target detection task. *Neuroimage*, *47*(4), 1532-1544. https://doi.org/10.1016/j.neuroimage.2009.05.082

Wilson, R. C., Takahashi, Y. K., Schoenbaum, G., & Niv, Y. (2014). Orbitofrontal cortex as a cognitive map of task space. *Neuron*, *81*(2), 267-279. https://doi.org/10.1016/j.neuron.2013.11.005

Woldorff, M. G., Hazlett, C. J., Fichtenholtz, H. M., Weissman, D. H., Dale, A. M., & Song, A. W. (2004). Functional parcellation of attentional control regions of the brain. *J Cogn Neurosci*, *16*(1), 149-165. https://doi.org/10.1162/089892904322755638

Woo, C.-W., Krishnan, A., & Wager, T. D. (2014). Cluster-extent based thresholding in fMRI analyses: pitfalls and recommendations. *NeuroImage*, *91*, 412-419.

Woolrich, M. W., Behrens, T. E. J., Beckmann, C. F., Jenkinson, M., & Smith, S. M. (2004). Multilevel linear modelling for FMRI group analysis using Bayesian inference. *NeuroImage*, *21*(4), 1732-1747. http://www.sciencedirect.com/science/article/pii/S1053811903007894

Worsley, K. J., Evans, A. C., Marrett, S., & Neelin, P. (1992). A three-dimensional statistical analysis for CBF activation studies in human brain. *Journal of Cerebral Blood Flow & Metabolism*, *12*(6), 900-918.

Yates, J. L., Park, I. M., Katz, L. N., Pillow, J. W., & Huk, A. C. (2017). Functional dissection of signal and noise in MT and LIP during decision-making. *Nat Neurosci*, *20*(9), 1285-1292. https://doi.org/10.1038/nn.4611

Yeo, B. T., Krienen, F. M., Sepulcre, J., Sabuncu, M. R., Lashkari, D., Hollinshead, M., Roffman, J. L., Smoller, J. W., Zollei, L., Polimeni, J. R., Fischl, B., Liu, H., & Buckner, R. L. (2011). The organization of the human cerebral cortex estimated by intrinsic functional connectivity. *J Neurophysiol*, *106*(3), 1125-1165. https://doi.org/10.1152/jn.00338.2011

Supplementary Information

System neglect and neurocomputational substrates for over- and underreactions to change

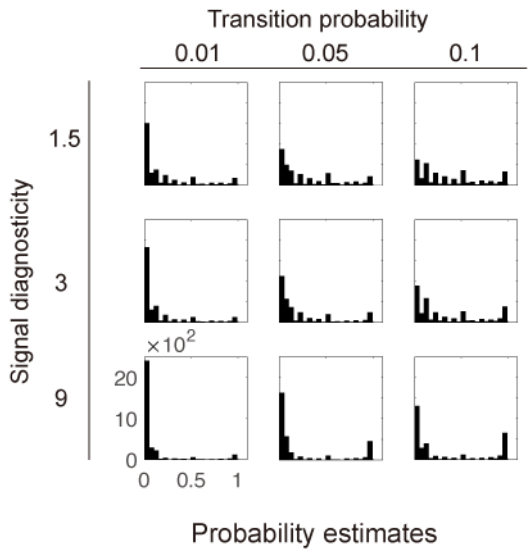

Figure S1. Probability estimates from all subjects are plotted as histograms separately for each condition. A condition is a combination of transition probability and signal diagnosticity.

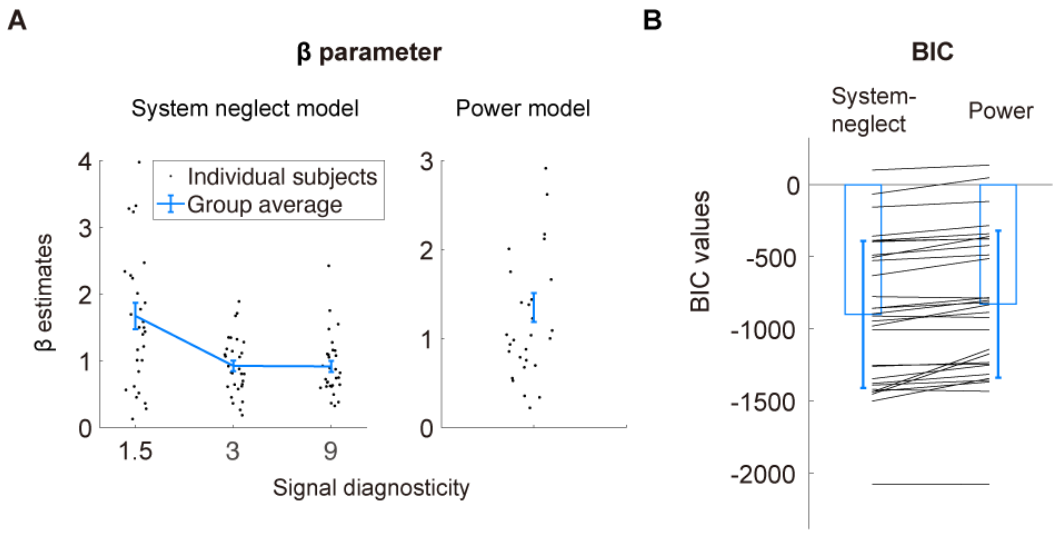

Figure S2. Experiment 2: model-fitting results. **A.** Weighting parameter for signal diagnosticity (β parameter) estimates of the two quasi-Bayesian models, the system-neglect model and the power model. **B.** Bayesian Information Criterion (BIC) of the system-neglect model and the power model. The bars indicate the mean BIC averaged across subjects. Each black line represents a single subject. Error bars represent 1 standard error of the mean. Lower BIC values indicate better models. BIC revealed that the system-neglect model was indeed the better model than the power model ($t(29) = 5.26$, $p < 0.01$). The BIC value was lower in the system-neglect model in 27 out of 30 subjects.

Robustness checks on the probability estimates of regime shifts (Fig. S3 to S5)

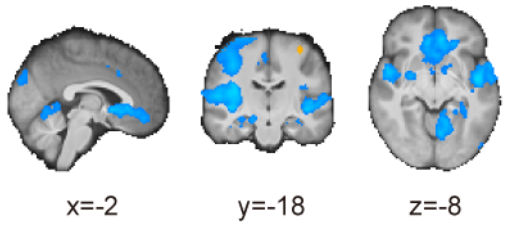

Figure S3. Whole-brain results on activity that significantly correlated with the subjects' log odds estimates of regime shift: $\log odds = \hat{P}/(1-\hat{P})$ where $\hat{P}$ is the subjects' probability estimates). In this analysis, we replaced the parametric regressor of $\hat{P}$ with the log odds of regime shifts in GLM-1. Blue: negative correlation, yellow: positive correlation. Familywise error-corrected at p<0.05 using Gaussian random field theory with a cluster-forming threshold z>3.1.

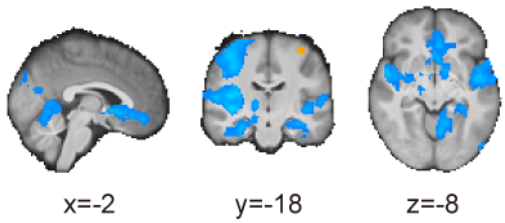

Figure S4. Whole-brain results on activity that significantly correlated with the subjects' probability estimates of regime shift ($\hat{P}$) in GLM-2. In GLM-2, we implemented variables important for estimating regime shifts as parametric regressors in addition to $\hat{P}$. Despite the fact that these variables correlating with $\hat{P}$, we still observed $\hat{P}$ correlates in the vmPFC and ventral striatum. Blue: negative correlation, yellow: positive correlation. Familywise error-corrected at p<0.05 using Gaussian random field theory with a cluster-forming threshold z>3.1.

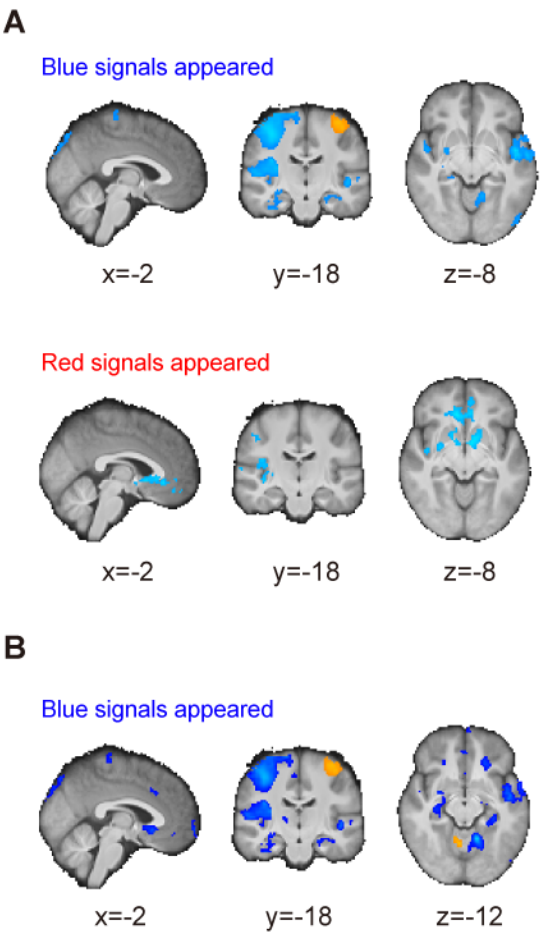

Figure S5. Probability estimates of regime shifts ($\hat{P}$) separately analyzed at the time the blue signals appeared and at the time the red signals appeared. **A.** Whole-brain results on activity that significantly correlated with the subjects' probability estimates of regime shift when blue signals appeared and red signals appeared. Blue: negative correlation, yellow: positive correlation. Familywise error-corrected at $p<0.05$ using Gaussian random field theory with a cluster-forming threshold $z>3.1$. **B.** Voxels ($p<0.001$ uncorrected) that correlated probability estimates when the blue signal appeared. We observed vmPFC to correlate with $\hat{P}$ at the time when red signals and when the blue signals appeared.

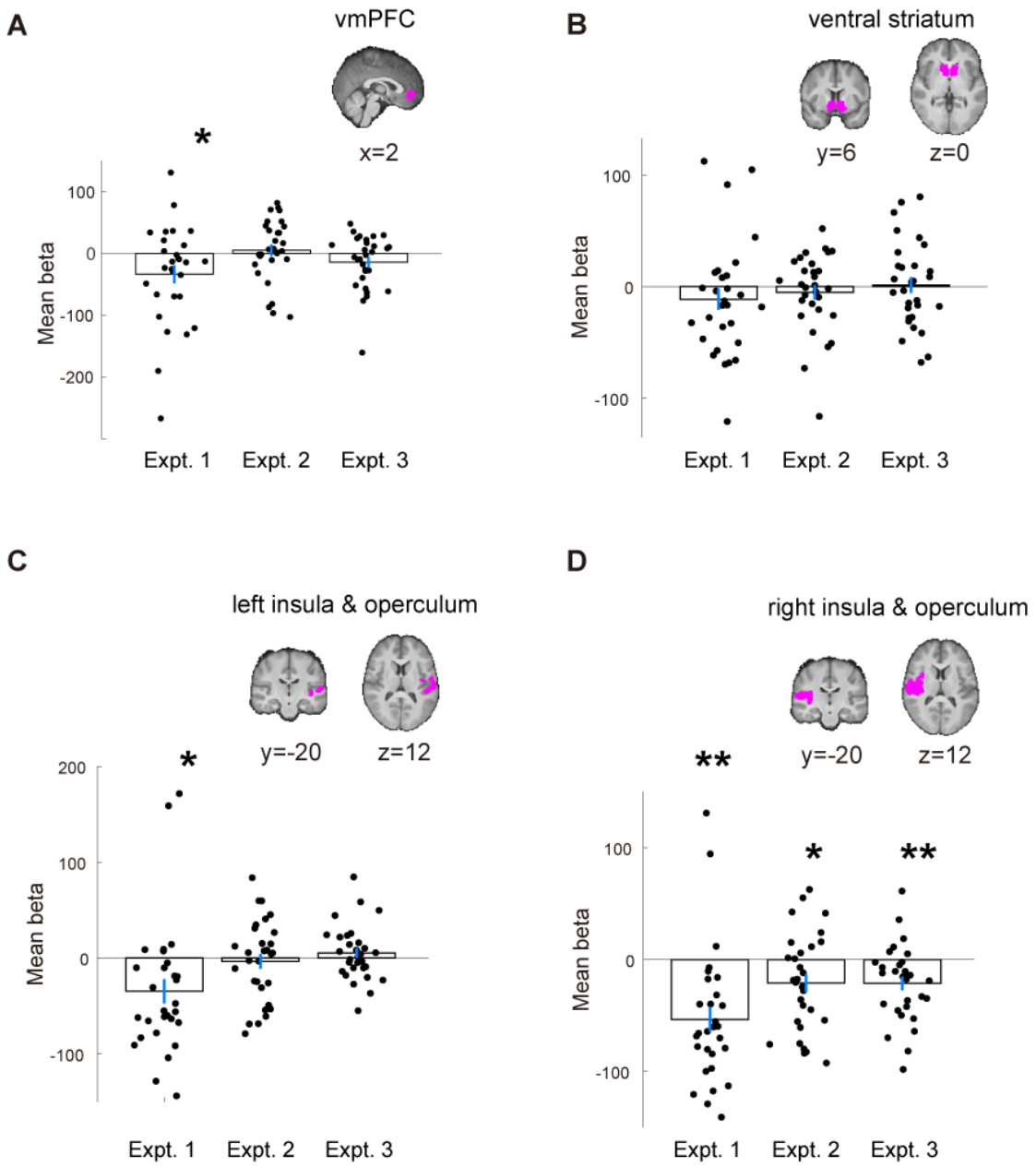

Figure S6. Independent region-of-interest (ROI) analysis. Neural representations for probability estimates across the three experiments. Only the probability estimates in Experiment 1 were about the estimates of regime shifts (see Methods in main texts). One outlier with extreme negative beta in Experiment 1 was excluded from the analysis. **A.** vmPFC mask from Bartra et al. (2013). Experiment 1: $t(28)=-2.38$, $p=0.02$; Experiment 2: $t(29)=0.56$, $p=0.58$; Experiment 3: $t(29)=-1.76$, $p=0.09$. **B.** Ventral striatum mask from Bartra et al. (2013). Experiment 1: $t(28)=1.88$, $p=0.07$; Experiment 2: $t(29)=-0.42$, $p=0.68$; Experiment 3: $t(29)=-0.74$, $p=0.46$). **C.** Left insula and operculum. Experiment 1: $t(28)=-2.71$, $p=0.01$; Experiment 2: $t(29)=-0.44$, $p=0.66$; Experiment 3: $t(29)=1.01$, $p=0.32$. **D.** Right insula and operculum. Experiment 1: $t(28)=-4.78$, $p<0.01$; Experiment 2: $t(29)=-2.63$, $p=0.01$; Experiment 3: $t(29)=-3.44$, $p<0.01$. The * symbol indicates $p<0.05$, and ** symbol indicates

$p<0.01$. Only the vmPFC and left insula extending to the operculum correlated with probability estimates in Experiment 1 but not in Experiments 2 and 3, further suggesting that these two regions uniquely represented probability estimates of regime shifts.

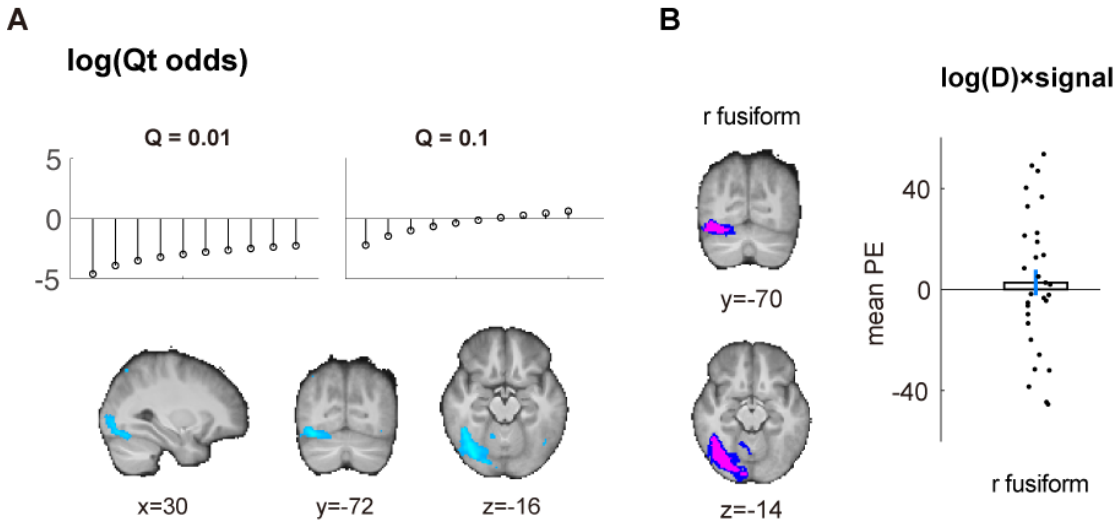

Figure S7. Key variables for regime-shift computations. **A.** Whole-brain results on the dynamic base rate of regime shift $\log(Q_t\ odds)$). **B.** Using the $\log(Q_t\ odds)$ ROI (left graph: magenta indicates voxels shared by the LOSO ROI of all subjects; blue indicates voxels of LOSO ROI of at least one subject) to examine the regression coefficients of log(D)×signal. The mean regression coefficient was not significant different from 0 ($t(29)=0.54$, $p=0.59$). The * symbol indicates $p<0.05$, ** indicates $p<0.01$.

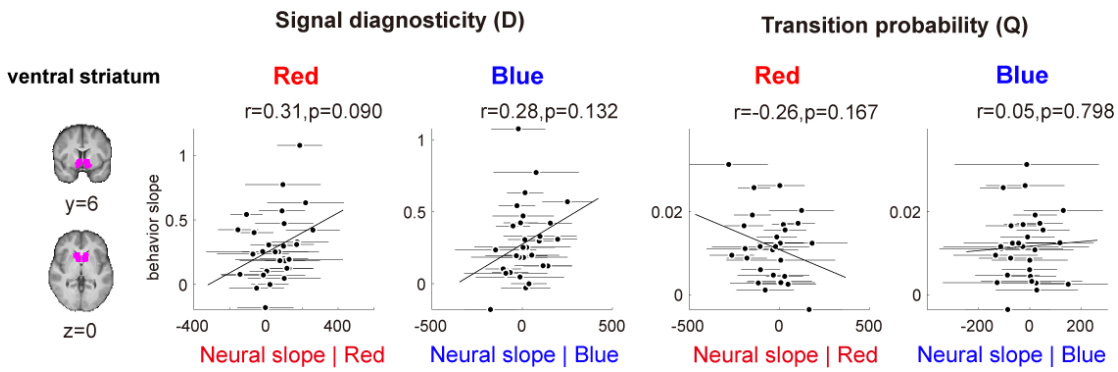

Figure S8. Individual subjects' degree of neglecting the system parameters in the ventral striatum.

Table S1. Experiment 1 GLM-1 Cluster-level inference using Gaussian random field theory (familywise error corrected at $p<0.05$ with a cluster-forming threshold $z>3.1$).

Probability estimates (negative correlation)				
Cluster	**Hemisphere**	**Cluster size**	**z-max**	**z-max(x,y,z)**
Parietal Operculum Cortex	R	8359	6.48	(50,-26,18)
Planum Polare	L	3250	5.33	(-48,-6,-8)
Occipital Pole	R	2355	5.59	(10,-88,40)
Subcallosal Cortex	-	1466	5.09	(0,14,-4)
Lingual Gyrus	L	1455	6.2	(-14,-52,-12)
Supplementary Motor Cortex	R	531	4.68	(12,0,48)
Probability estimates (positive correlation)				
Postcentral Gyrus	L	1680	5.45	(-46,-26,56)

Table S2. Experiment 1: GLM-1. Permutation tests based on threshold-free-cluster-enhancement (TFCE) statistic.

Probability estimates (negative correlation)				
Cluster	**Hemisphere**	**Cluster size**	**1-p_{max}**	**1-p_{max}(x,y,z)**
Occipital Pole	R	5265	0.998	(12,-100,24)
Postcentral Gyrus	R	2420	1	(38,-20,44)
Planum Polare	R	1346	0.98	(60,-4,4)
Middle Temporal Gyrus, anterior division	L	767	0.986	(-62,-4,-10)
Subcallosal Cortex	-	399	0.973	(0,12,-4)
Lingual Gyrus	L	284	0.965	(-16,-52,-16)
Temporal Pole	L	217	0.966	(-52,18,-22)
Temporal Pole	R	2	0.95	(26,10,-28)
Probability estimates (positive correlation)				
Precentral Gyrus	L	1241	0.999	(-40,-26,56)

Table S3. Experiment 1: GLM-1. Permutation tests based on cluster extent.

Probability estimates (negative correlation)				
Cluster	**Hemisphere**	**Cluster size**	**1-p_{max}**	**1-p_{max}(x,y,z)**
Postcentral Gyrus	R	1690	1	(44,-18,36)
Occipital Pole	R	778	0.998	(16,-106,0)
Occipital Pole	-	437	0.993	(0,-104,12)
Superior Temporal Gyrus, posterior division	R	435	0.993	(66,-22,8)
Middle Temporal Gyrus, anterior division	L	240	0.985	(-60,0,-16)
Frontal Orbital Cortex	L	203	0.982	(-12.36,-20)
Lateral Occipital Cortex, superior division	L	163	0.977	(-52,-76,28)
Occipital Pole	L	161	0.976	(-40,-94,10)
Heschl's Gyrus	R	150	0.974	(56,-10,4)
Lateral Occipital Cortex, inferior division	R	142	0.972	(60,-68,-4)
Middle Temporal Gyrus, anterior division	R	87	0.956	(40,4,-30)
Probability estimates (positive correlation)				
Supramarginal Gyrus, anterior division	L	1541	0.999	(-44,-30,38)

Table S4. Experiment 2: GLM-1. Cluster-level inference using Gaussian random field theory (familywise error corrected at $p<0.05$ with a cluster-forming threshold $z>3.1$).

Probability estimates (negative correlation)				
Cluster	**Hemisphere**	**Cluster size**	**z-max**	**z-max(x,y,z)**
Postcentral Gyrus	R	3208	5.3	(40,-26,52)
Temporal Occipital Fusiform Cortex	L	956	5.7	(-22,-52,-22)
Parietal Operculum Cortex	R	407	5.37	(50,-20,22)
Probability estimates (positive correlation)				
Postcentral Gyrus	L	504	4.07	(-44,-22,68)

Table S5. Experiment 3: GLM-1. Cluster-level inference using Gaussian random field theory (familywise error corrected at $p<0.05$ with a cluster-forming threshold $z>3.1$).

Probability estimates (negative correlation)				
Cluster	Hemisphere	Cluster size	z-max	z-max(x,y,z)
Parietal Operculum Cortex	R	8359	6.48	(50,-26,18)
Planum Polare	L	3250	5.33	(-48,-6,-8)
Occipital Pole	R	2355	5.59	(10,-88,40)
Subcallosal Cortex	-	1466	5.09	(0,14,-4)
Lingual Gyrus	L	1455	6.2	(-14,-52,-12)
Supplementary Motor Cortex	R	531	4.68	(12,0,48)
Probability estimates (positive correlation)				
Postcentral Gyrus	L	1680	5.45	(-46,-26,56)

Table S6. Experiment 1: GLM-2. Cluster-level inference using Gaussian random field theory (familywise error corrected at $p<0.05$ with a cluster-forming threshold $z>3.1$).

Probability estimates (negative correlation)				
Cluster	Hemisphere	Cluster size	z-max	z-max(x,y,z)
Lingual Gyrus	L	11504	6.2	(-14,-52,-12)
Central Opercular Cortex	R	9872	6.19	(60,-8,6)
Probability estimates (positive correlation)				
Postcentral Gyrus	L	1680	5.45	(-46,-26,56)
Belief update (positive correlation)				
Left Cerebral White Matter	L	717	4.33	(-20,18,-12)
Cingulate Gyrus, anterior division	-	566	4.39	(0,32,-8)
Frontal Orbital Cortex	R	475	4.17	(20,8,-16)
Postcentral Gyrus	L	333	4.02	(-30,-28,64)
Log(Qt_odds) (negative correlation)				
Occipital Fusiform Gyrus	R	1833	4.61	(36,-74,-16)
Lateral Occipital Corte	R	223	4.04	(36,-66,-56)
Lateral Occipital Cortex	L	204	4.25	(-40,-82,-8)
Log(D) × signal (positive correlation)				
Middle Frontal Gyrus	R	988	4.17	(36,10,30)
Superior Frontal Gyrus	R	821	4.56	(6,34,48)
Superior Parietal Lobule	L	620	4.26	(-40,-52,56)
Supramarginal Gyrus	R	604	4.29	(46,-40,48)
Middle Frontal Gyrus	L	277	4.21	(-46,34,30)

Table S7. Experiment 1: GLM-2. Permutation tests based on the threshold-free-cluster-enhancement (TFCE) statistic.

Probability estimates (negative correlation)				
Cluster	Hemisphere	Cluster size	$1\text{-}p_{max}$	$1\text{-}p_{max}(x,y,z)$
Postcentral Gyrus	R	31490	1	(38,-24,50)
Frontal Pole	R	165	0.962	(16,36,-20)
Probability estimates (positive correlation)				
Postcentral Gyrus	L	439	0.988	(-42,-28,54)
Belief update (positive correlation)				
Right Caudate	R	2857	0.973	(12,14,-4)
Cingulate Gyrus, anterior division	R	1873	0.973	(4,26,24)
Postcentral Gyrus	L	707	0.966	(-42,-22,54)
Insular Cortex	L	427	0.959	(-42,6,-4)
Frontal Medial Cortex	L	320	0.96	(-4,40,-14)
Frontal Pole	L	40	0.952	(-2,60,28)
Insular Cortex	R	20	0.952	(40,6,-14)
Log(Qt_odds) (negative correlation)				
Lateral Occipital Cortex, inferior division	R	2117	0.994	(38,-74,14)
Frontal Pole	R	185	0.962	(36,42,36)
Frontal Pole	R	114	0.957	(40,44,-6)
Middle Frontal Gyrus	R	14	0.952	(34,28,50)
Right Thalamus	R	13	0.954	(22,-28,-2)
Frontal Pole	R	1	0.95	(32,48,-8)
Frontal Pole	R	1	0.95	(30,52,-6)

Table S8. Experiment 1 GLM-2. Permutation tests based on cluster extent

Probability estimates (negative correlation)				
Cluster	Hemisphere	Cluster size	$1\text{-}p_{max}$	$1\text{-}p_{max}(x,y,z)$
Postcentral Gyrus	R	1770	0.999	(42,-20,38)
Lateral Occipital Cortex, inferior division	R	1085	0.997	(60,-68,-6)
Lateral Occipital Cortex, inferior division	L	674	0.994	(-42,-84,10)
Temporal Fusiform Cortex, posterior division	L	597	0.993	(-36,-18,-32)
Heschl's Gyrus	R	527	0.992	(54,-12,2)
Temporal Fusiform Cortex, anterior division	R	441	0.99	(34,-2,-30)
Cerebellar Left V	L	235	0.978	(-16,-50,-24)
Middle Temporal Gyrus, anterior division	L	193	0.973	(-52,-4-18)
Frontal Medial Cortex	L	134	0.961	(-10,34,-18)
Lingual Gyrus	L	134	0.961	(-6,-48,-2)
Probability estimates (positive correlation)				
Supramarginal Gyrus, anterior division	L	1012	0.998	(-44,-30,40)
Belief update (positive correlation)				
Cingulate Gyrus, anterior division	-	450	0.984	(0,34,14)
Frontal Orbital Cortex	R	351	0.979	(16,12,-16)
Frontal Orbital Cortex	L	300	0.976	(-22,10,-18)
Postcentral Gyrus	L	215	0.965	(-38,-24,46)
Log(Qt odds) (negative correlation)				
Temporal Occipital Fusiform Cortex	R	1687	0.998	(34,-60,24)
Lateral Occipital Cortex, superior division	R	220	0.958	(38,-70,32)

Log(D) × signal (positive correlation)				
Superior Parietal Lobule	L	384	0.978	(-38,-52,40)

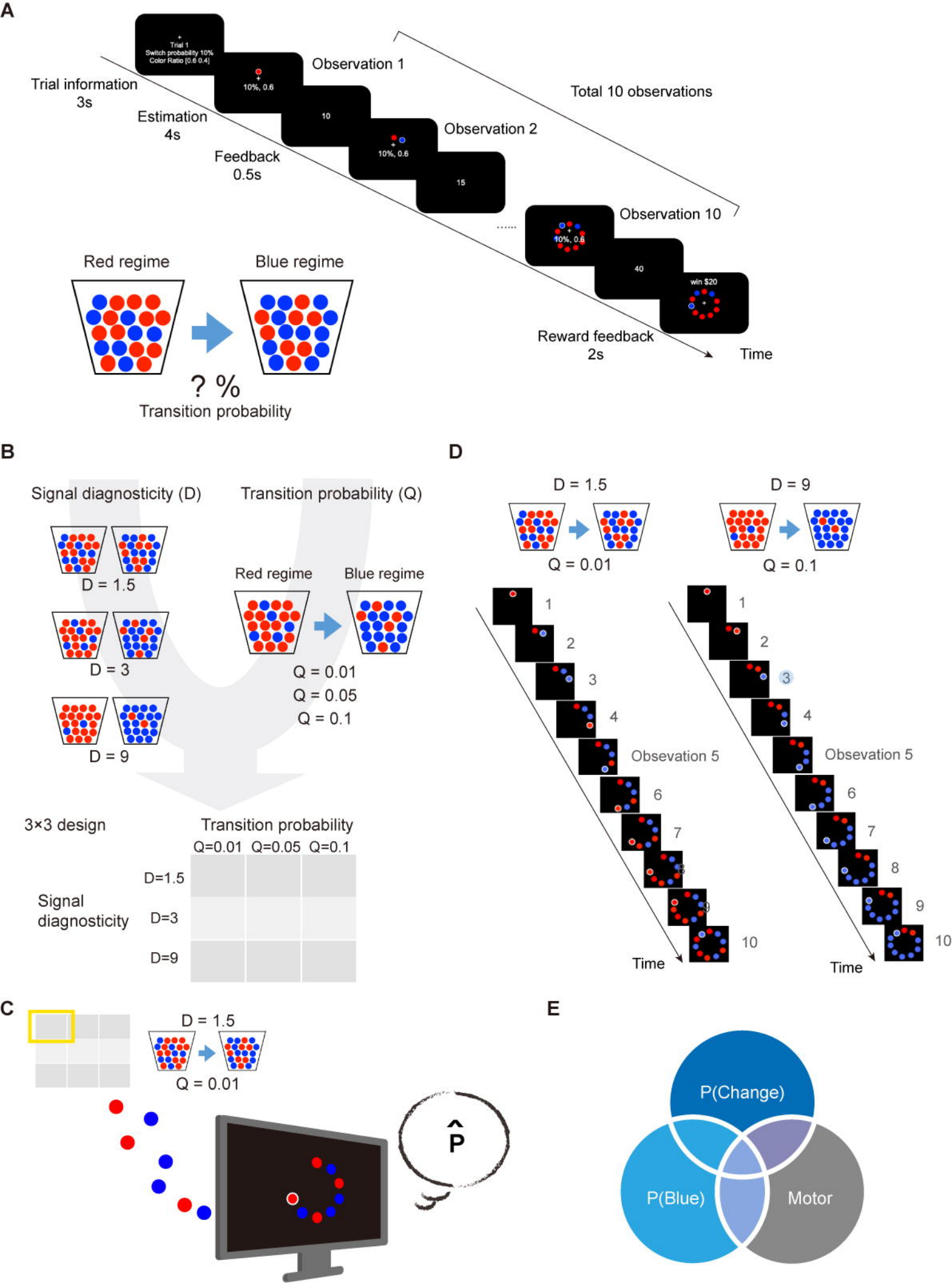
A
Trial 1
Switch probability 10%
Color Ratio [0.6 0.4]
10%, 0.6
10
10%, 0.6
15
10%, 0.6
40
win $20
Trial information
3s
Estimation
4s
Feedback
0.5s
Observation 1
Observation 2
Observation 10
Total 10 observations
Reward feedback
2s
Time
Red regime
Blue regime
? %
Transition probability
B
Signal diagnosticity (D)
Transition probability (Q)
D = 1.5
D = 3
D = 9
Red regime
Blue regime
Q = 0.01
Q = 0.05
Q = 0.1
3×3 design
Transition probability
Q=0.01 Q=0.05 Q=0.1
Signal diagnosticity
D=1.5
D=3
D=9
D
D = 1.5
Q = 0.01
D = 9
Q = 0.1
1
2
3
4
Obsevation 5
6
7
8
9
10
Time
C
D = 1.5
Q = 0.01
P̂
E
P(Change)
P(Blue)
Motor

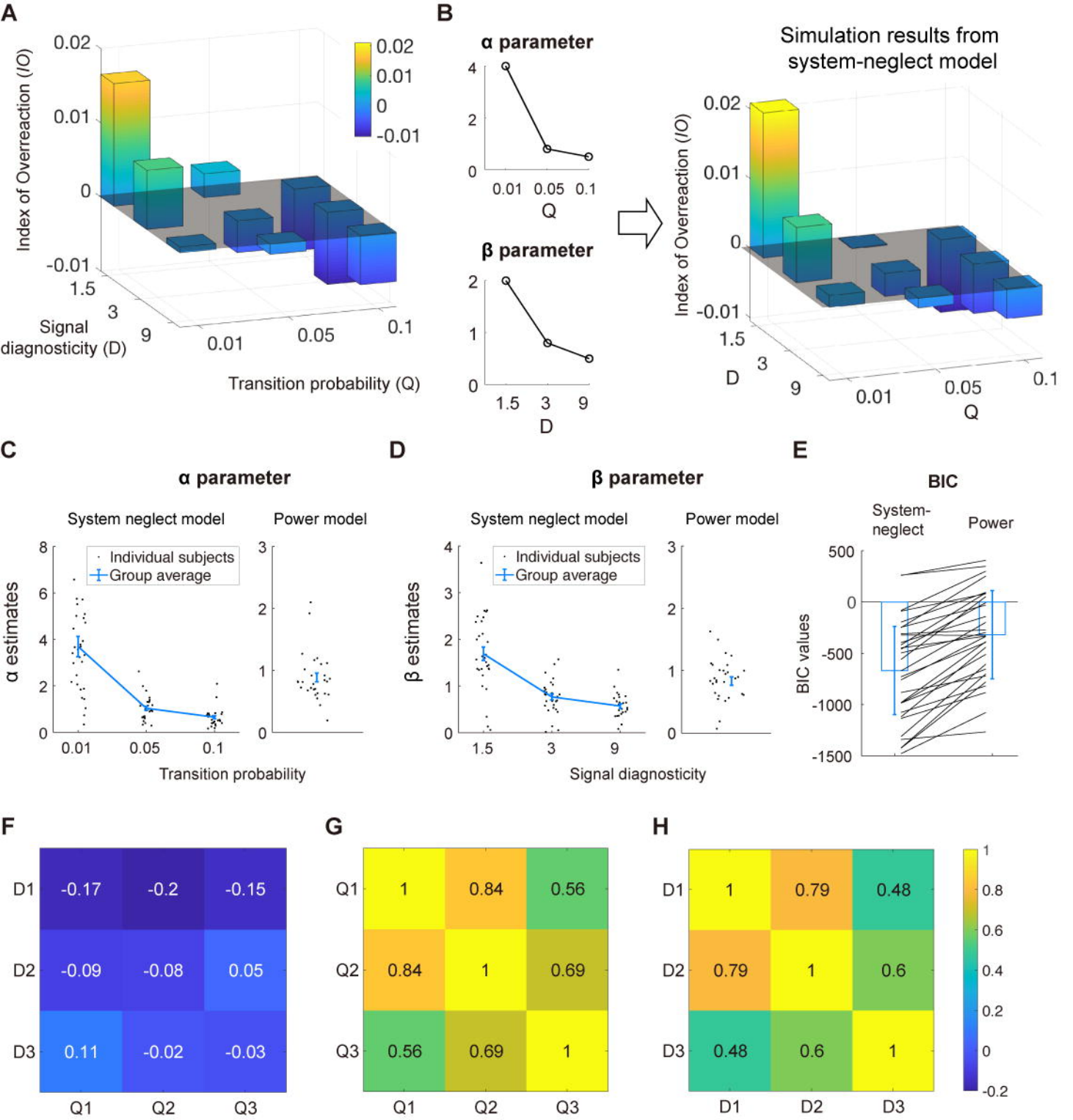
A
Index of Overreaction (IO)
0.02
0.01
0
-0.01
1.5
3
9
Signal diagnosticity (D)
0.01
0.05
0.1
Transition probability (Q)
B
α parameter
β parameter
Q
D
Simulation results from system-neglect model
C
α parameter
System neglect model
Power model
Individual subjects
Group average
α estimates
Transition probability
D
β parameter
β estimates
Signal diagnosticity
E
BIC
System-neglect
Power
BIC values
F
D1 -0.17 -0.2 -0.15
D2 -0.09 -0.08 0.05
D3 0.11 -0.02 -0.03
Q1 Q2 Q3
G
Q1 1 0.84 0.56
Q2 0.84 1 0.69
Q3 0.56 0.69 1
H
D1 1 0.79 0.48
D2 0.79 1 0.6
D3 0.48 0.6 1

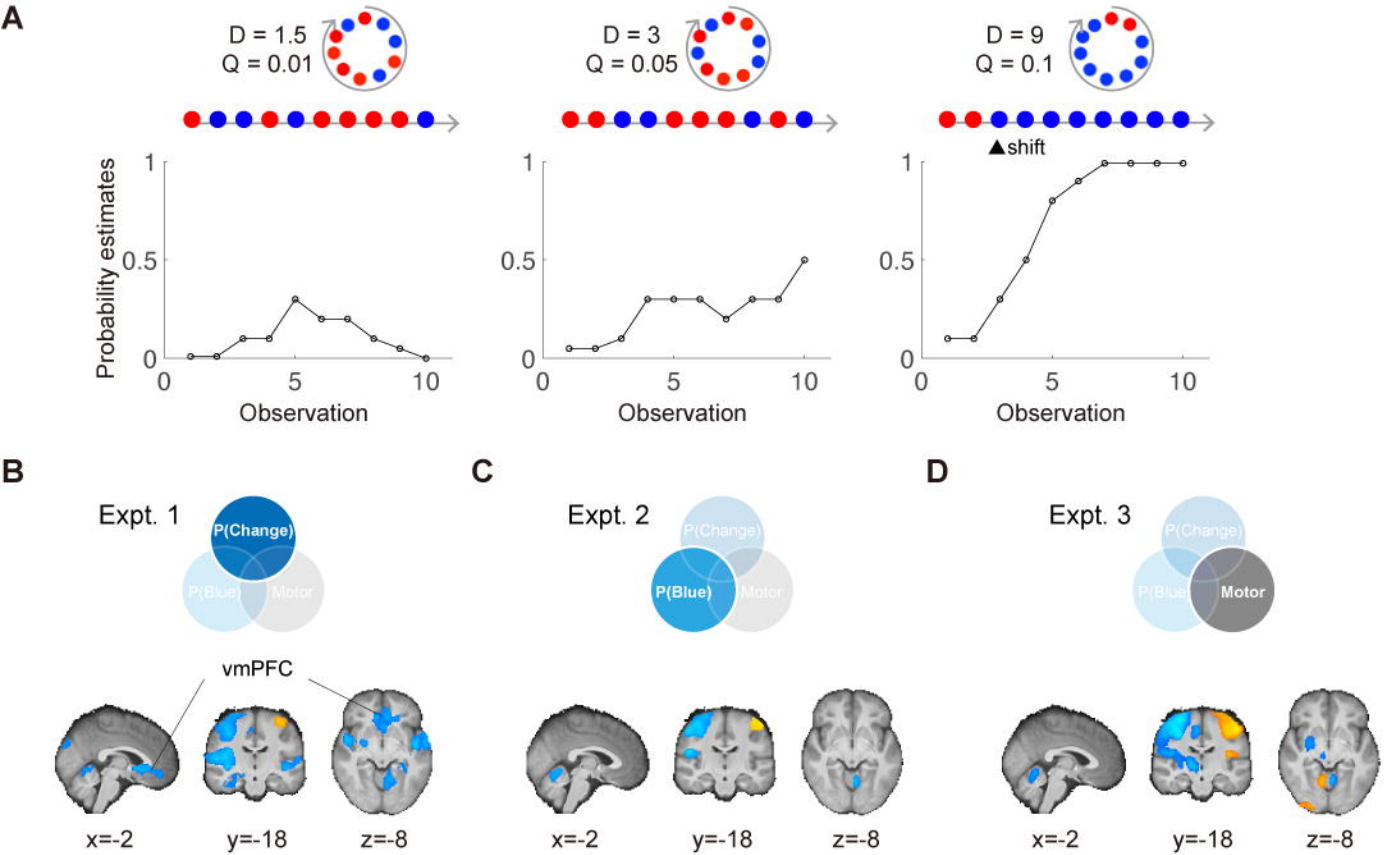
A
D = 1.5
Q = 0.01
D = 3
Q = 0.05
D = 9
Q = 0.1
▲shift
Probability estimates
Observation
B
Expt. 1
P(Change)
P(Blue)
Motor
vmPFC
x=-2
y=-18
z=-8
C
Expt. 2
P(Change)
P(Blue)
Motor
x=-2
y=-18
z=-8
D
Expt. 3
P(Change)
P(Blue)
Motor
x=-2
y=-18
z=-8

A

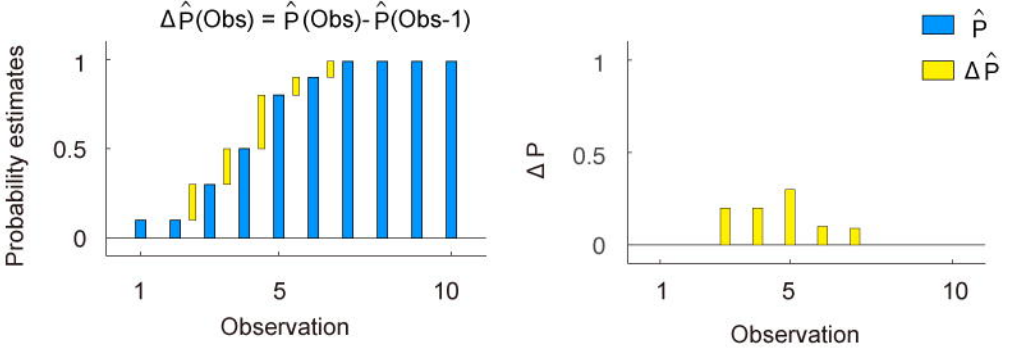
$\Delta\hat{P}(Obs) = \hat{P}(Obs) - \hat{P}(Obs-1)$
Probability estimates
1
0.5
0
1
5
10
Observation
ΔP
1
0.5
0
1
5
10
Observation
$\hat{P}$
$\Delta\hat{P}$

B

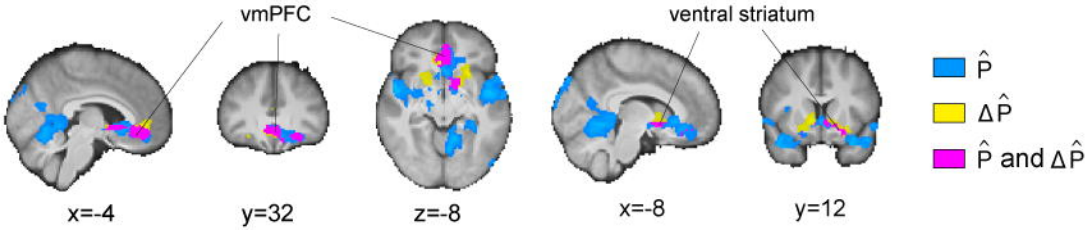
vmPFC
ventral striatum
x=-4
y=32
z=-8
x=-8
y=12
$\hat{P}$
$\Delta\hat{P}$
$\hat{P}$ and $\Delta\hat{P}$

A

log(D)×signal

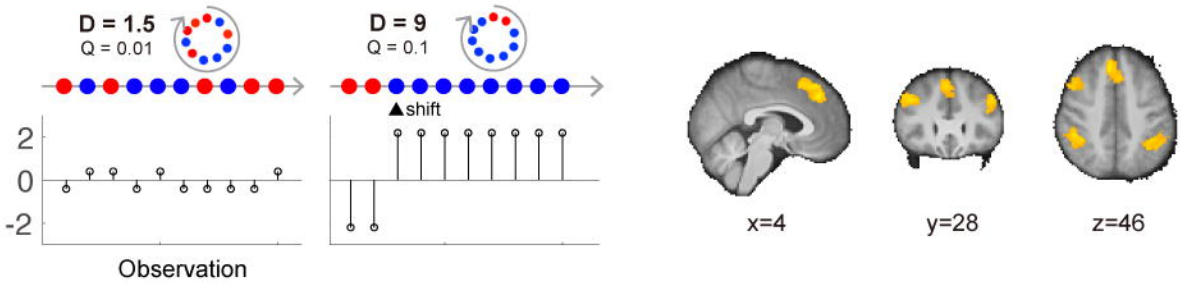

B

log(Qt odds)

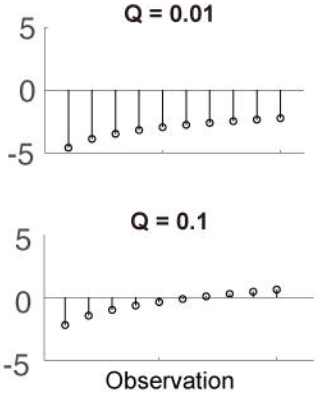

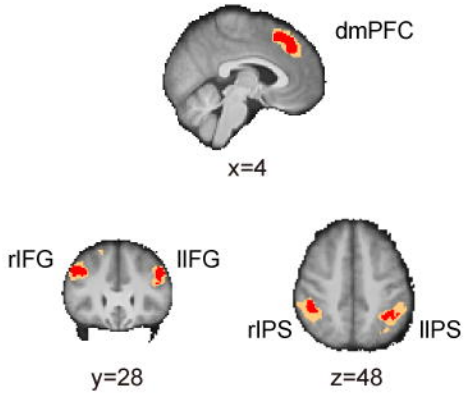

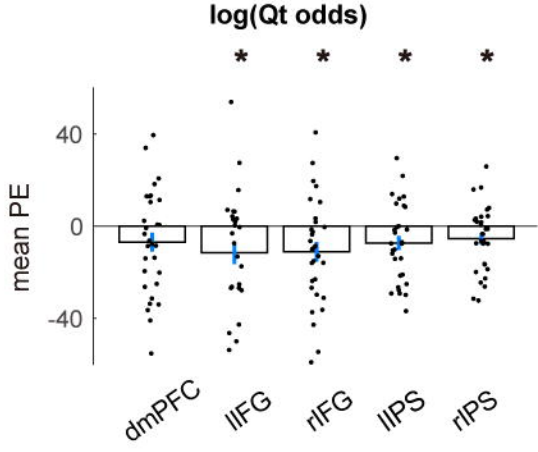

A

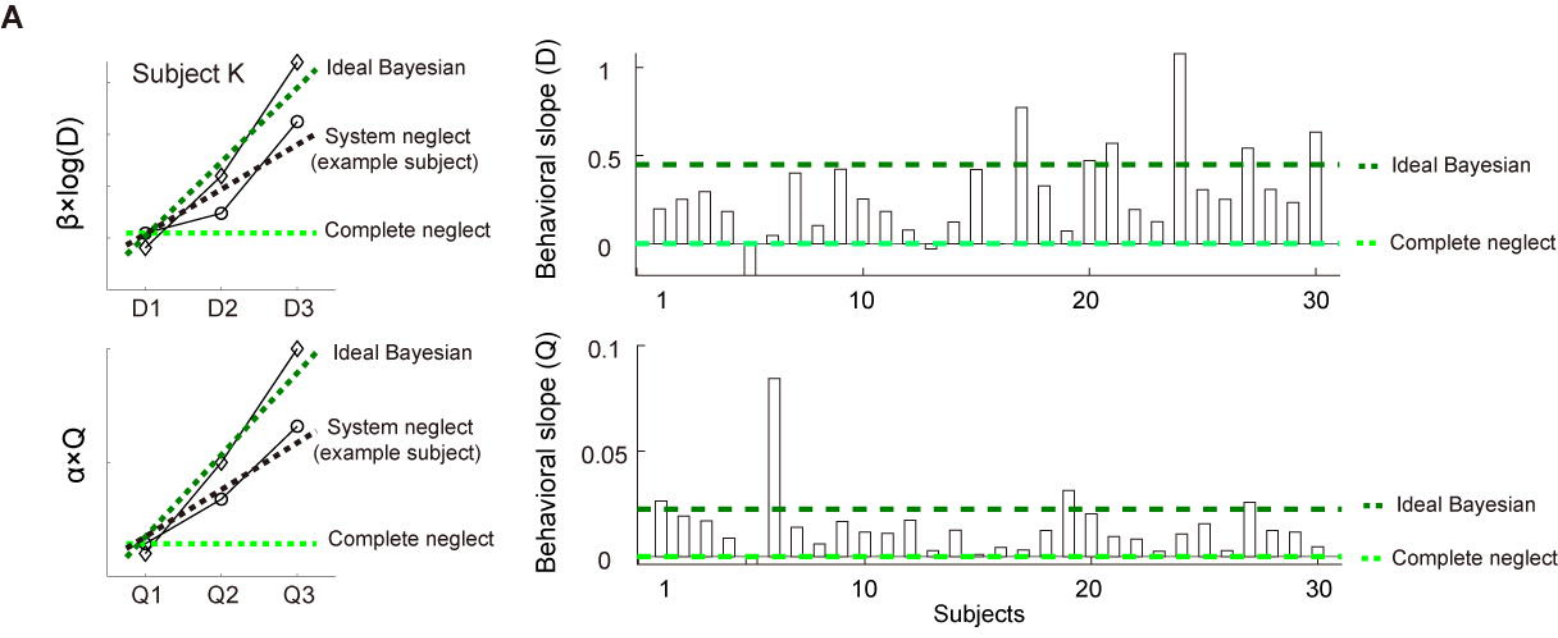
Subject K
Ideal Bayesian
System neglect
(example subject)
Complete neglect
β×log(D)
D1
D2
D3
α×Q
Q1
Q2
Q3
Behavioral slope (D)
Behavioral slope (Q)
Subjects

B

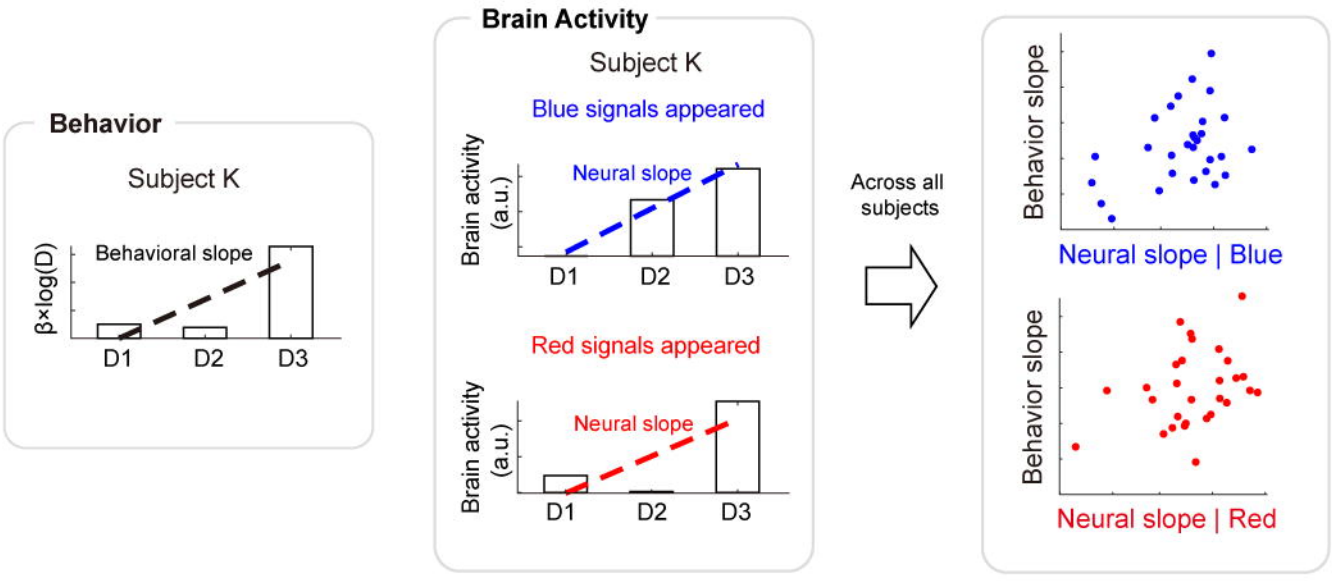
Behavior
Subject K
Behavioral slope
β×log(D)
D1
D2
D3
Brain Activity
Subject K
Blue signals appeared
Neural slope
Brain activity (a.u.)
Red signals appeared
Across all subjects
Behavior slope
Neural slope | Blue
Neural slope | Red

C

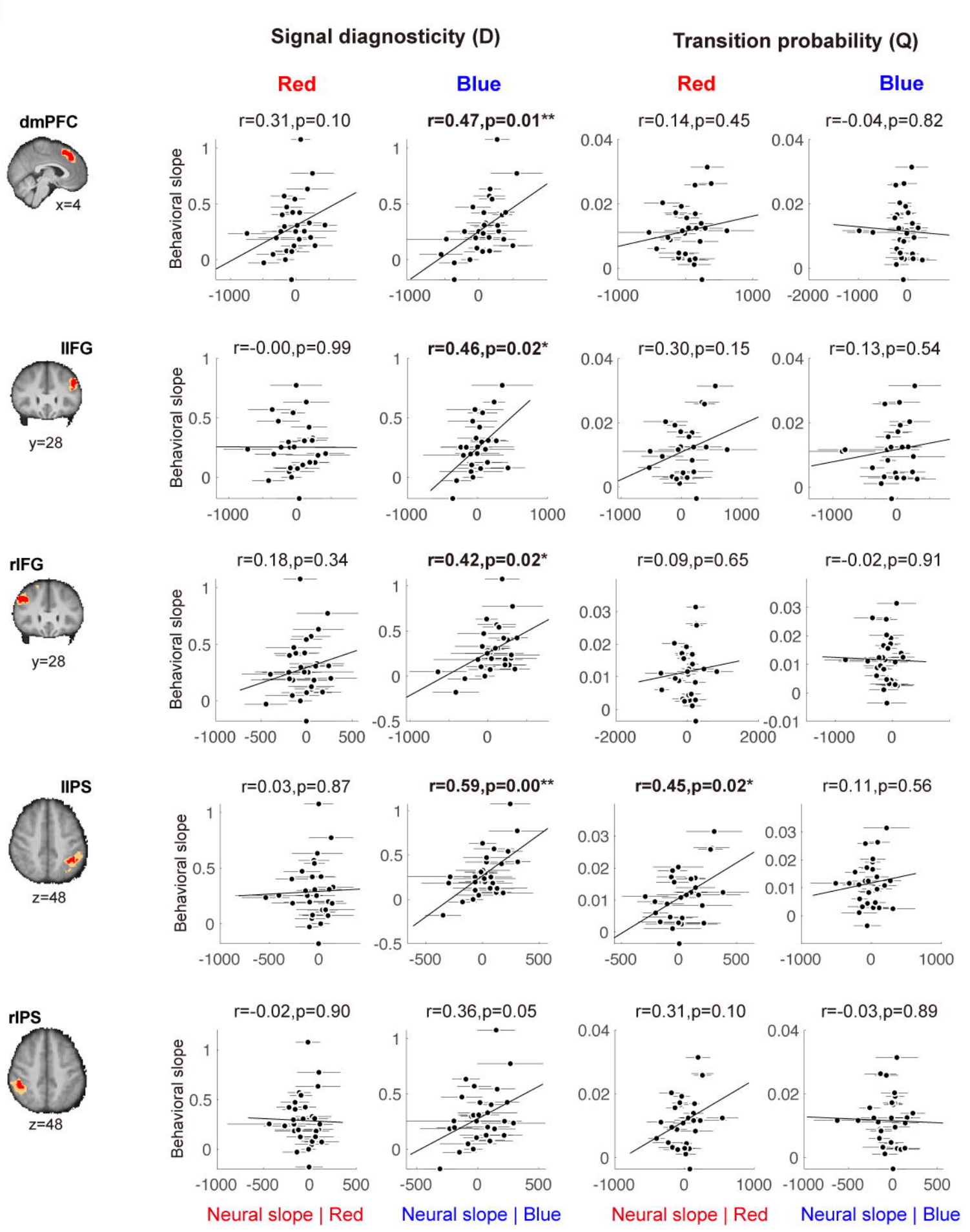
Signal diagnosticity (D)
Transition probability (Q)
Red
Blue
dmPFC
x=4
r=0.31,p=0.10
r=0.47,p=0.01**
r=0.14,p=0.45
r=-0.04,p=0.82
lIFG
y=28
r=-0.00,p=0.99
r=0.46,p=0.02*
r=0.30,p=0.15
r=0.13,p=0.54
rIFG
y=28
r=0.18,p=0.34
r=0.42,p=0.02*
r=0.09,p=0.65
r=-0.02,p=0.91
lIPS
z=48
r=0.03,p=0.87
r=0.59,p=0.00**
r=0.45,p=0.02*
r=0.11,p=0.56
rIPS
z=48
r=-0.02,p=0.90
r=0.36,p=0.05
r=0.31,p=0.10
r=-0.03,p=0.89
Behavioral slope
Neural slope | Red
Neural slope | Blue

D

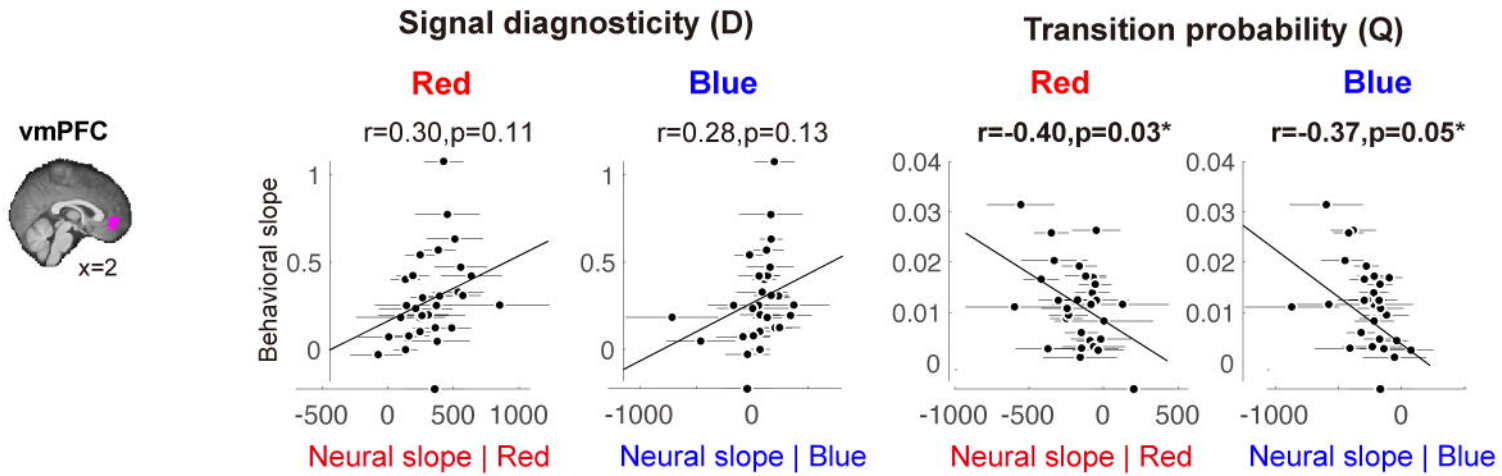
Signal diagnosticity (D)
Transition probability (Q)
Red
Blue
vmPFC
x=2
r=0.30,p=0.11
r=0.28,p=0.13
r=-0.40,p=0.03*
r=-0.37,p=0.05*
Behavioral slope
Neural slope | Red
Neural slope | Blue

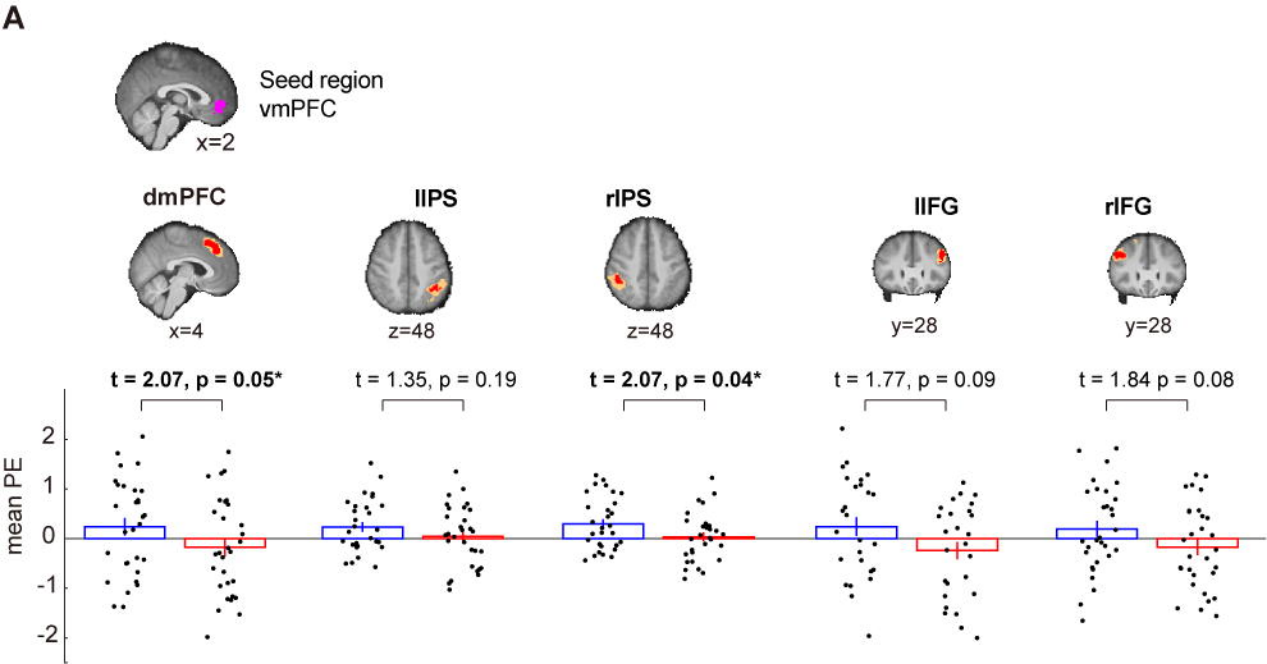
A
Seed region
vmPFC
x=2
dmPFC
x=4
lIPS
z=48
rIPS
z=48
lIFG
y=28
rIFG
y=28
t = 2.07, p = 0.05*
t = 1.35, p = 0.19
t = 2.07, p = 0.04*
t = 1.77, p = 0.09
t = 1.84 p = 0.08
mean PE
2
1
0
-1
-2

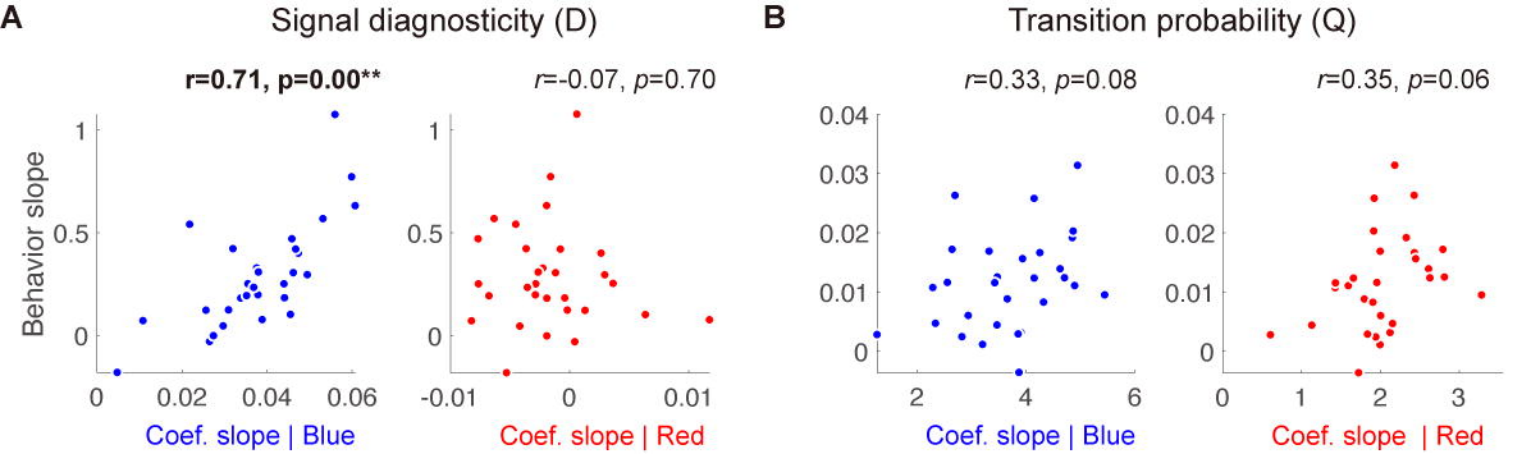
A
Signal diagnosticity (D)
r=0.71, p=0.00**
r=-0.07, p=0.70
Behavior slope
1
0.5
0
0
0.02
0.04
0.06
-0.01
0
0.01
Coef. slope | Blue
Coef. slope | Red
B
Transition probability (Q)
r=0.33, p=0.08
r=0.35, p=0.06
0.04
0.03
0.02
0.01
0
2
4
6
0
1
2
3
Coef. slope | Blue
Coef. slope | Red